



OAK RIDGE NATIONAL LABORATORY

operated by

UNION CARBIDE CORPORATION

for the

U.S. ATOMIC ENERGY COMMISSION



OAK RIDGE NATIONAL LABORATORY LIBRARIES



3 4456 0549997 5

ORNL - TM - 1400

DECLASSIFIED

CLASSIFICATION CHANGED TO

BY AUTHORITY OF AECM-2104 a2 B6 8/21/24

BY: BL Rudd

FUELS AND MATERIALS DEVELOPMENT PROGRAM QUARTERLY PROGRESS

REPORT FOR PERIOD ENDING DECEMBER 31, 1965

Compiled by

P. Patriarca

OAK RIDGE NATIONAL LABORATORY
 CENTRAL RESEARCH LIBRARY
 CIRCULATION SECTION
 4500N ROOM 175

LIBRARY LOAN COPY

DO NOT TRANSFER TO ANOTHER PERSON.
if you wish someone else to see this report, send in
name with report and the library will arrange a loan.

ORNL-118 (6-97)

NOTICE This document contains information of a preliminary nature
and was prepared primarily for internal use at the Oak Ridge National
Laboratory. It is subject to revision or correction and therefore does
not represent a final report.

LEGAL NOTICE

This report was prepared as an account of Government sponsored work. Neither the United States, nor the Commission, nor any person acting on behalf of the Commission:

- A. Makes any warranty or representation, expressed or implied, with respect to the accuracy, completeness, or usefulness of the information contained in this report, or that the use of any information, apparatus, method, or process disclosed in this report may not infringe privately owned rights; or
- B. Assumes any liabilities with respect to the use of, or for damages resulting from the use of any information, apparatus, method, or process disclosed in this report.

As used in the above, "person acting on behalf of the Commission" includes any employee or contractor of the Commission, or employee of such contractor, to the extent that such employee or contractor of the Commission, or employee of such contractor prepares, disseminates, or provides access to, any information pursuant to his employment or contract with the Commission, or his employment with such contractor.

Contract No. W-7405-eng-26

FUELS AND MATERIALS DEVELOPMENT PROGRAM QUARTERLY PROGRESS
REPORT FOR PERIOD ENDING DECEMBER 31, 1965

Compiled by

P. Patriarca

FEBRUARY 1966

OAK RIDGE NATIONAL LABORATORY
Oak Ridge, Tennessee
operated by
UNION CARBIDE CORPORATION
for the
U. S. ATOMIC ENERGY COMMISSION

OAK RIDGE NATIONAL LABORATORY LIBRARIES



3 4456 0549997 5

[Redacted]

[Redacted]

FOREWORD

This is the seventh quarterly progress report describing work performed at the Oak Ridge National Laboratory for the Fuels and Materials Branch, Division of Reactor Development and Technology, U. S. Atomic Energy Commission. The specific programs covered are as follows:

Part I. Metals and Ceramics Division

<u>Program Title</u>	<u>Person in Charge</u>	<u>Principal Investigator(s)</u>
Controlled Precipitation in Nuclear Materials	W. C. Harms	J. L. Scott J. P. Hammond
Fuel Element Development	G. M. Adamson, Jr.	C. F. Leitten, Jr.
Mechanical Properties	D. A. Douglas, Jr.	J. R. Weir, Jr.
Nondestructive Test Development	D. A. Douglas, Jr.	R. W. McClung
Zirconium Metallurgy	C. J. McHargue	M. L. Picklesimer

Part II. Reactor Chemistry Division

Fission-Gas Release and Physical Properties of Fuel Materials During Irradiation	O. Sisman	R. M. Carroll M. F. Osborne
---	-----------	--------------------------------

[REDACTED]

[REDACTED]

TABLE OF CONTENTS

	Page
Summary	vii
Part I. Metals and Ceramics Division	
1. Controlled Precipitation in Nuclear Materials	3
Effect of Dispersed Precipitates on the Properties of Ceramic Materials	3
Precipitation Studies in Alumina	3
Growth of Titanium-Doped Al ₂ O ₃ Single Crystals	4
Dispersion Strengthening of Metals by Controlled Precipitation	5
Aluminum Alloys	5
Thorium Alloys	8
2. Fuel Element Development	13
Deposition of Uranium Dioxide by Hydroreduction of Uranium Hexafluoride	13
Deposition of Uranium Dioxide by Hydroreduction of Uranium Tetrachloride	15
Deposition of Uranium Compounds by Lithium Vapor Reduction of Uranium Hexafluoride	16
Deposition of Tungsten Alloys	18
Deposition of Molybdenum	20
3. Mechanical Properties	22
Irradiation Embrittlement in Titanium-Bearing Type 304 Stainless Steel	22
Mechanical Properties of Titanium-Modified Type 304 Stainless Steel	24
Postirradiation Creep and Stress-Rupture of Type 304 Stainless Steel	28
Elevated-Temperature Embrittlement of Structural Material Welds and Brazes	30
4. Nondestructive Test Development	33
Electromagnetic Test Methods	33
Analytical Studies	33
Phase-Sensitive Eddy-Current Instrument	34

Ultrasonic Test Methods	34
Nonbond Studies	34
Tubing Inspection	36
Schlieren System	36
Penetrating Radiation	39
X- and Gamma-Ray Attenuation Gaging	39
5. Zirconium Metallurgy	41
Deformation, Creep, and Fracture in Alpha-Zirconium Alloys	41
Research on the Mechanical Anisotropy of Zircaloy-2	42
Effects of Neutron Irradiation and Vacuum Annealing on Oxide Films on Zirconium	42
Anisotropy in Zircaloy-2	43
Zircaloy-2 Tubing	43
Correlation of Yield Strengths with the "k" Values and Texture	46
Determination of Yield Surfaces	47
Oxide Film Studies	50
Purification of Zirconium	50
Preparation of Single Crystals of Zirconium and Its Alloys	51
Properties of High-Purity Zirconium	51
Oxidation	51
Hydrides in Zirconium	53

Part II. Reactor Chemistry Division

6. Fission-Gas Release and Physical Properties of Fuel Materials During Irradiation	60
Uranium Dioxide Single-Crystal Specimen, Cl-18	60
Fission-Gas Release (Steady State)	62
Low-Temperature Release	62
High-Temperature Release	65
Oscillations of Neutron Flux	70
Temperature Oscillations	70
Gas-Transfer Functions	70

[REDACTED]

SUMMARY

1. Controlled Precipitation in Nuclear Materials

Controlled precipitation of 0.1% TiO_2 in Al_2O_3 is being studied as a possible technique for improving the work-to-fracture of Al_2O_3 . A superior product would have both nuclear and nonnuclear applications. In previous work crack-free, titania-doped alumina single crystals were produced, but they contained undesirable bubbles. By careful control of flame chemistry, geometry, and temperature we have recently grown pure Al_2O_3 single crystals without cracks or bubbles: The process is now being extended to titania doped crystals. An extension of the work involving doping of polycrystalline Al_2O_3 by heating in contact with Ti_2O_3 was initiated.

In another phase of the work controlled precipitates of cerium and yttrium intermetallic compounds are being introduced into aluminum by the SLIS process in an effort to produce dispersion hardening. Shortcomings of the horizontal-jet SLIS technique were observed and two new SLIS techniques are being investigated. The SLIS technique was used to produce precipitates of a beryllium-thorium compound in thorium. A Th-1.3 wt % Be alloy was successfully prepared by the horizontal-jet technique and was extruded to wrought rod form. Hot-hardness tests, a criterion of elevated-temperature strength, gave DPH values over three times as high as unalloyed thorium at 600 and 750°C.

2. Fuel Element Development

Studies in this period consisted mainly in refining the several processes being investigated for direct conversion of uranium halides to high-temperature fuels. Fabrication behavior of UO_2 powders produced from UF_6 appears to be similar to those produced by the ADU process. Conversion of UCl_4 to UO_2 has been carried out at higher feed rates to obtain sufficient material for further evaluation.

The lithium vapor reduction of UF_6 to uranium metal has been successfully demonstrated; however, a better method for control of lithium vapor flow remains to be developed before the technique can be applied to fabrication of compounds such as UC or UN.

Work in the codeposition of tungsten and rhenium from their respective fluorides indicates that homogeneous alloying can be reproduced for lengths of tubing for testing or for further fabrication.

3. Mechanical Properties

We have continued to investigate the elevated-temperature radiation-induced embrittlement of stainless steels. Our objectives in this part of the program are to determine the mechanism for the damage and to attempt to alleviate the problem by metallurgical treatment of the material prior to irradiation.

Recent results of postirradiation tensile testing of type 304 stainless steel, modified by the addition of 0.2% Ti, have shown the alloy to be much superior to type 304 stainless steel after irradiation at 700°C to 10^{21} neutrons/cm² (thermal). Transmission electron micrography of irradiated specimens has revealed that no helium bubbles form in the titanium-bearing steel whereas for the same conditions grain-boundary bubbles are found in type 304 stainless steel.

Postirradiation creep-rupture tests of type 304 stainless steel at 650°C show that preirradiation heat treatment in the temperature range from 800 to 900°C produces significantly better properties than the standard 1036°C anneal. These results are consistent with our observations from postirradiation tensile tests.

We have recently begun investigations of radiation damage in welds and brazes of type 304 stainless steel and Inconel 600. Initial results indicate that the mechanical properties of welds and brazes are significantly affected by irradiation.

4. Nondestructive Test Development

We are developing new techniques and equipment for the nondestructive evaluation of materials and components. The major emphasis has been on eddy-current, ultrasonic, and penetrating-radiation methods.

[REDACTED]

The mathematical approach using a computer to analyze variations in electromagnetic field parameters has been applied to the calculation of the mechanical force generated by eddy currents. Improvements have been made to the phase-sensitive eddy-current instrument to obtain better stability.

The ultrasonic program has continued to work on techniques for nonbond evaluation. A remotely controlled method has been successfully applied to fuel tubes in a hot cell. Our work on reference standards is being extended to circumferential electrodischarge machined notches. We have assembled a Schlieren system and are developing techniques to allow optical visualization of ultrasonic energy.

Our scintillation gaging work has concentrated on the calibration variables for fuel rod scanning.

5. Zirconium Metallurgy

Three papers were presented at a Symposium on Zirconium and its Alloys at the 1965 Fall Meeting of the Electro chemical Society in Buffalo, New York, October 10-14, 1965. They are entitled, "Deformation, Creep, and Fracture in Alpha-Zirconium Alloys," "Research on the Mechanical Anisotropy of Zircaloy-2," and "Effects of Neutron Irradiation and Vacuum Annealing on Oxide Films on Zirconium." Abstracts of these papers are presented.

Four lots of Zircaloy-2 tubing have been received from vendors. One lot has received preliminary examination. The texture has essentially a random distribution of basal poles between the radial and tangential directions.

Attempts to correlate yield strengths in tension and compression with "k" values of strain anisotropy have been only moderately successful. One function has been found which is useful but not completely satisfactory.

Flow surfaces on the octahedral plane of stress space have been developed by the hardness-anisotropy method for several lots of Zircaloy-2 plate on which there was a large amount of other mechanical property data. The fit with experimental data is good for some textures of material but poor for others.

[REDACTED]

A variable range electrometer has been used to measure the room-temperature electrical conductivity of anodized and air-formed oxide films on zirconium specimens. The conductivity of the air-formed films was greater, consistent with the previous conclusion that it contained a greater concentration of defects as observed by optical absorption.

Anisotropy of oxidation in air with crystallographic direction in the thicker film stage has been examined on a single-crystal sphere of zirconium. The oxidation rate can vary by a factor as large as 4 in less than 20° of crystallographic angle. Similar anisotropy of oxide formation by anodization in 1% KOH has been shown but by at most a factor of 2 at low voltages and by 1.2 at higher voltages. At anodization voltages above 50 the oxidation anisotropy is reversed in comparison to that at voltages less than 50.

Hydrides in slowly cooled high-purity zirconium have been found to be optically anisotropic, indicating that their crystal structure is not cubic. Hydrides have been observed to have habit planes differing from $\{10\bar{1}0\}$ as well as $\{10\bar{1}0\}$. A chemical polishing and an electro-polishing solution have been developed that do not preferentially attack either the matrix or the hydride particle.

6. Fission-Gas Release and Physical Properties of Fuel Materials During Irradiation

Thin-disk specimens of UO_2 are being irradiated for the purpose of developing a model for fission-gas release. In these experiments the specimen may be irradiated at different flux levels and independently controlled temperatures. Fission gas is removed by a sweep gas and the release rate from the UO_2 specimen is determined by gamma-spectrometry.

A defect-trap model has been developed and steady-state and oscillating tests are being made to evaluate the model. At this time, polished single-crystal specimens are compared with unpolished single-crystal specimens. The gas release from the polished single-crystal specimens shows results which we believe are caused by fission generated clusters of point defects. The clusters cause the fission-gas release rate to be influenced by the temperature history of the specimen, an effect not observed before.

[REDACTED]

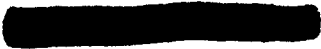
The effects of oscillation frequency were studied showing that, at high temperatures, the magnitude of the fission-gas release was not influenced by the frequency of temperature or fission-rate oscillation.

The mixing of fission gas in the sweep gas was studied to find how well the fission-gas release waves could be resolved.

[REDACTED]

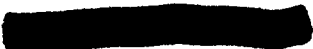
[REDACTED]

[REDACTED]



PART I.

METALS AND CERAMICS DIVISION



[REDACTED]

[REDACTED]

1. CONTROLLED PRECIPITATION IN NUCLEAR MATERIALS

J. L. Scott

J. P. Hammond

The purpose of this program is to investigate means for improving the performance of both fissionable and nonfissionable materials by optimizing the microstructure through controlled precipitation of stable, dispersed phases.

Effect of Dispersed Precipitates on the Properties
of Ceramic MaterialsPrecipitation Studies in Alumina - D. I. Matkin¹

Studies were continued to evaluate the effect of whisker-shaped precipitates on crack propagation in single-crystal and polycrystalline alumina. The immediate aim is to produce by suitable heat treatment a homogeneous distribution of precipitates in titanium-doped single crystals and subsequently polycrystalline Al_2O_3 .

Difficulties have been encountered in obtaining titanium-doped Al_2O_3 single crystals that are free of both bubbles and cracks.² Attempts have been made to ameliorate these difficulties by (a) diffusing titanium into defect-free, pure Al_2O_3 single crystals and (b) modifying the growing conditions in an effort to improve the quality of the crystals.

Thermodynamic calculations indicated that Ti_2O_3 should be the stable oxide of titanium at 1700°C in reasonably dry hydrogen. Since one would expect Ti^{3+} to be the fastest diffusing ion of titanium in the corundum (Al_2O_3) structure, attempts have been made to increase the diffusion of titanium into single crystals by annealing the crystals in contact with Ti_2O_3 in hydrogen at 1700°C. The effectiveness of this treatment is being evaluated by laser microprobe chemical analysis.

¹On loan from AERE, Harwell, England.

²D. I. Matkin, Fuels and Materials Development Program Quart. Progr. Rept. Sept. 30, 1965, ORNL-TM-1270, pp. 3-5.

As an extension to the single-crystal program, initial precipitation studies have been made on pressed and sintered pellets of Al_2O_3 containing 1% Ti_2O_3 . The pellets were subsequently heat treated at a variety of temperatures and times in both air and hydrogen atmospheres. Evaluation of these pellets is in progress.

Growth of Titanium-Doped Al_2O_3 Single Crystals - D. I. Matkin,
J. Y. Chang,³ G. W. Clark

We have continued to study modifications to the growing conditions in an effort to improve the quality of titanium-doped single crystals of Al_2O_3 grown by flame fusion.

The necessary flame conditions for crystal growth by the flame-fusion technique appear to be correct temperature, correct flame geometry to give uniform growth conditions and to minimize thermal shock, and correct flame chemistry to maintain chemical stability of the growing crystal. It is difficult to make independent changes in temperature, flame geometry, and flame chemistry, because the controlling parameters are interdependent. However, we have changed the flame geometry by reducing the internal diameter of the furnace muffle from 1 1/2 to 3/4 in. (see Fig. 1.1, ref. 2). The flow of oxygen and hydrogen in the flame is now more streamlined and this has extended the length of the flame thus reducing thermal gradients and thermal shock.

It has been established by studying changes in the flame chemistry that it is possible to grow pure Al_2O_3 single crystals free of bubbles with a slightly oxygen-rich, oxyhydrogen flame. Under these conditions, however, Ti_2O_3 present in the doped powder used for growing doped crystals would have a tendency to oxidize to TiO_2 , giving rise to bubbles in the doped crystal. The temperature of the flame is also dependent upon the oxygen-to-hydrogen ratio and so it still remains to determine the optimum ratio to grow bubble-free, titanium-doped Al_2O_3 crystals.

³Consultant, Department of Chemical and Metallurgical Engineering, University of Tennessee.

Dispersion Strengthening of Metals by
Controlled Precipitation

J. P. Hammond

Aluminum Alloys

Several aluminum-base alloy powders containing cerium and yttrium and prepared by the horizontal-jet SLIS technique,⁴ described in detail elsewhere,^{5,6} have been received from Nuclear Metals, Inc. These early runs were not entirely successful because not all of the solute was retained in supersaturated solid solution during quenching. The powders served a very useful purpose, however, in pointing the way to improved SLIS techniques and providing a means for gaining experience in powder handling and fabricating techniques.

Alloys of Al-3 at. % Ce, Al-2 at. % Ce, and Al-2 at. % Y were supplied as 3- to 5-lb batches of powder. Some physical characteristics of the systems involved and pertinent properties of the solutes are presented in Table 1.1. The values reported indicate that the systems and alloys selected are attractive for application of the SLIS process.

The microstructure of the Al-2% Ce alloy after cold pressing at 25 tsi is shown in Fig. 1.1 and is representative of those for the other two cold-pressed alloys. The area shown in Fig. 1.1 was selected to clearly show the individual powder particles and does not reflect the density achievable by cold pressing. It is apparent that a large portion of the material was not effectively quenched; in fact, for all three alloys, less than 50 vol % of the particles were precipitate-free after the horizontal-jet SLIS operation. Major problems in this connection are believed to be the following: (1) The atomized particles were not sufficiently small to ensure effective quenching on collision with the

⁴A method of preparing particles of supersaturated solid solutions by quenching molten particles containing a solute that is soluble in the liquid state but insoluble in the solid state.

⁵J. P. Hammond, Fuels and Materials Development Program Quart. Progr. Rept. Sept. 30, 1965, ORNL-TM-1270, pp. 5-6.

⁶A. R. Kaufman and W. C. Muller, Development of Zirconium-Base Alloys Strengthened by SLIS Technique, NMI-1263 (Jan. 15, 1965).

Table 1.1. Properties of Aluminum-Cerium and Aluminum-Yttrium Systems Used in SLIS Studies

	Aluminum-Cerium	Aluminum-Yttrium
Eutectic Reaction		
Composition, at. %	2.0 ^a	3.3 ^b
Temperature, °C	638 ^a	650 ^b
Solubility of Solute at 500°C	None detected ^{a,c}	d
Constitution of Precipitate	CeAl ₄ ^a	YAl ₃ ^b
Goldschmidt Atomic Diameter, A		
Solute	3.64 ^e	3.62 ^e
Aluminum	2.80-2.85 ^e	2.80-2.85 ^e
Thermal Neutron Absorption		
Cross Section of Solute, barns	0.73 ± 0.08 ^f	1.31 ± 0.08 ^f

^aM. Hansen, Constitution of Binary Alloys, McGraw-Hill Book Co., Inc., 1958.

^bJ. A. McGurty, Constitution of Yttrium Alloys, DC 59-5-210, May 19, 1959.

^cBased on lattice-parameter method.

^dNot determined but probably very low in view of differences in atomic diameters, electronegativity, and crystal structure of solute and solvent.

^eL. S. Darken and R. W. Gurry, Physical Chemistry of Metals, McGraw-Hill Book Co., Inc., 1953.

^fBrookhaven National Laboratory Report No. 325, 2nd ed.

quenching disk and (2) many particles did not hit the disk because of poor directional control of the fan-shaped spray emanating from the argon jet.

Another problem apparently inherent in the horizontal-jet method stems from difficulties during die loading due to the fluffy and resilient character of the material; frequent tamping and use of an extension tube were necessary in order to obtain adequate loading. Operations were

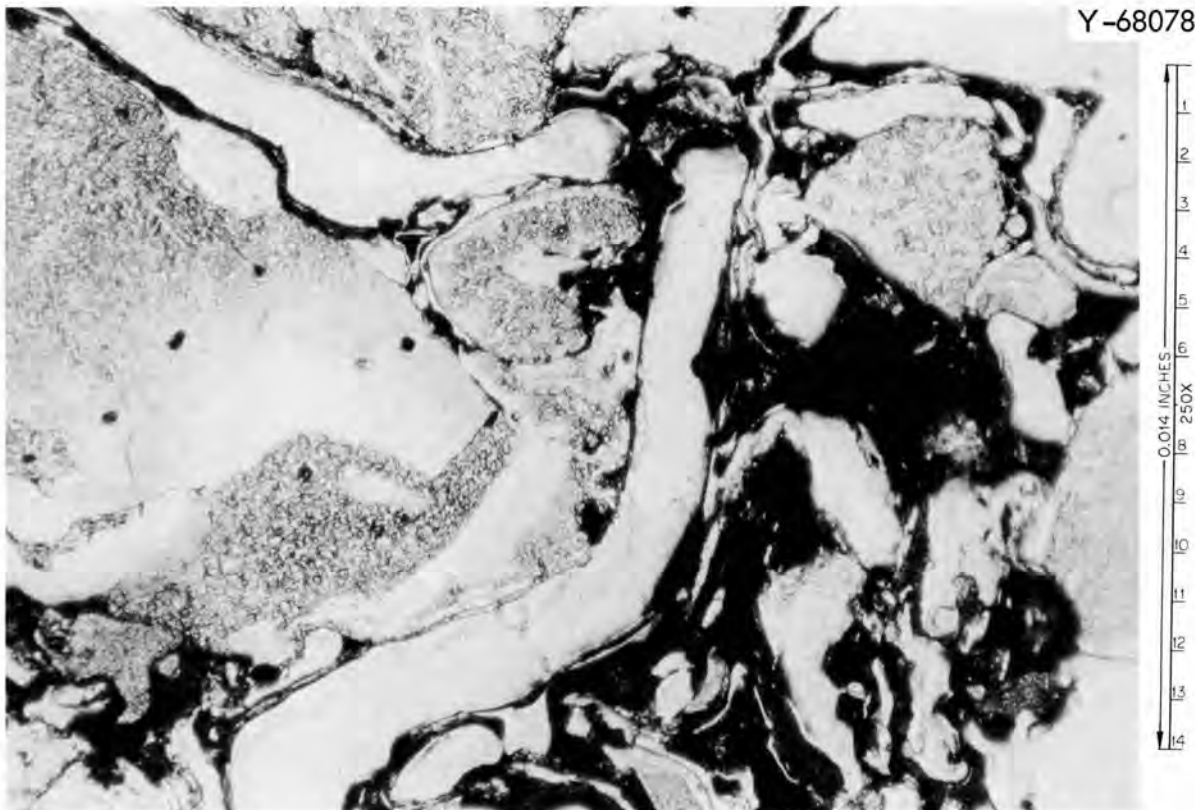


Fig. 1.1. Photomicrograph of Al-2 at. % Ce Alloy Compact Prepared from SLIS Powder by Cold Pressing at 25 tsi-Pressure. Effectively quenched material is represented by the clear, precipitate-free areas. Electrolytically etched in 15 parts ethyl alcohol to 1 part perchloric acid.

generally carried out in an argon-filled dry box, although the powders were nonpyrophoric and could be handled in air.

Compacts of the Al-3% Ce alloy prepared from the inadequately quenched powders were cold pressed at 50 tsi and upset-extruded at a 9-to-1 reduction ratio at 480°C. The hot hardness of the resulting product was determined to 600°C and was found to be inferior to that for an XAP-1000 alloy (SAP with 6% Al₂O₃) fabricated in a similar manner.

In view of the difficulties cited above with the material prepared by the horizontal-jet method, two additional SLIS techniques were investigated. One involves "capillary blowing" of the molten alloy through a refractory glass capillary, obliquely against a small rotating

quenching wheel. In the second method the material is atomized, prior to quenching on a large rotating wheel, by consumably arc melting the alloy as a 2-in.-diam anode as it rotates at high velocity. By comparison with the horizontal-jet technique, both methods give a finer product and provide better directional control of the atomized material.

Material prepared by each of the three SLIS methods is shown in Fig. 1.2 (A, B, and C), along with ball-milled products from the horizontal-jet (D) and capillary-blown (E) techniques. The ball-milled products gave a much higher tapped density and were far easier to load into dies. The physical appearance of the powder prepared by the spinning-anode process (C) suggests that this product may give favorable dispensing and pressing characteristics without the milling step.

Thorium Alloys

Dispersion-hardened thorium-base alloys of two principal descriptions were hot extruded to rod form and evaluated by hot-hardness testing from room temperature to 800°C. The first of these was a Th-1.3 wt % Be alloy prepared as a powder by the horizontal-jet SLIS process and subsequently upset-extruded at 600°C to form a 1-in.-diam rod. The second category of material represents early efforts to dispersion harden thorium-zirconium solid-solution alloys by forming a fine precipitate of the stable ZrB₂ compound by internal boronation during fabrication. In this technique, elemental boron is finely distributed in a compact of the thorium-zirconium alloy powder and diffusion-reacted during preliminary consolidation by hot pressing or, alternatively, cold pressing and sintering. The boronated compacts were hot extruded at 750°C to 3/8-in.-diam rod. The results of hot hardness tests on these materials are given in Table 1.2 along with data for arc-cast unalloyed thorium and an arc-cast Th-5 wt % Zr alloy,⁷ shown to be the most attractive arc-cast alloyed material in earlier work, for comparison.

⁷J. A. Burka and J. P. Hammond, Evaluation of Thorium-Base Alloys for High-Temperature Strength, ORNL-3777 (April 1965).

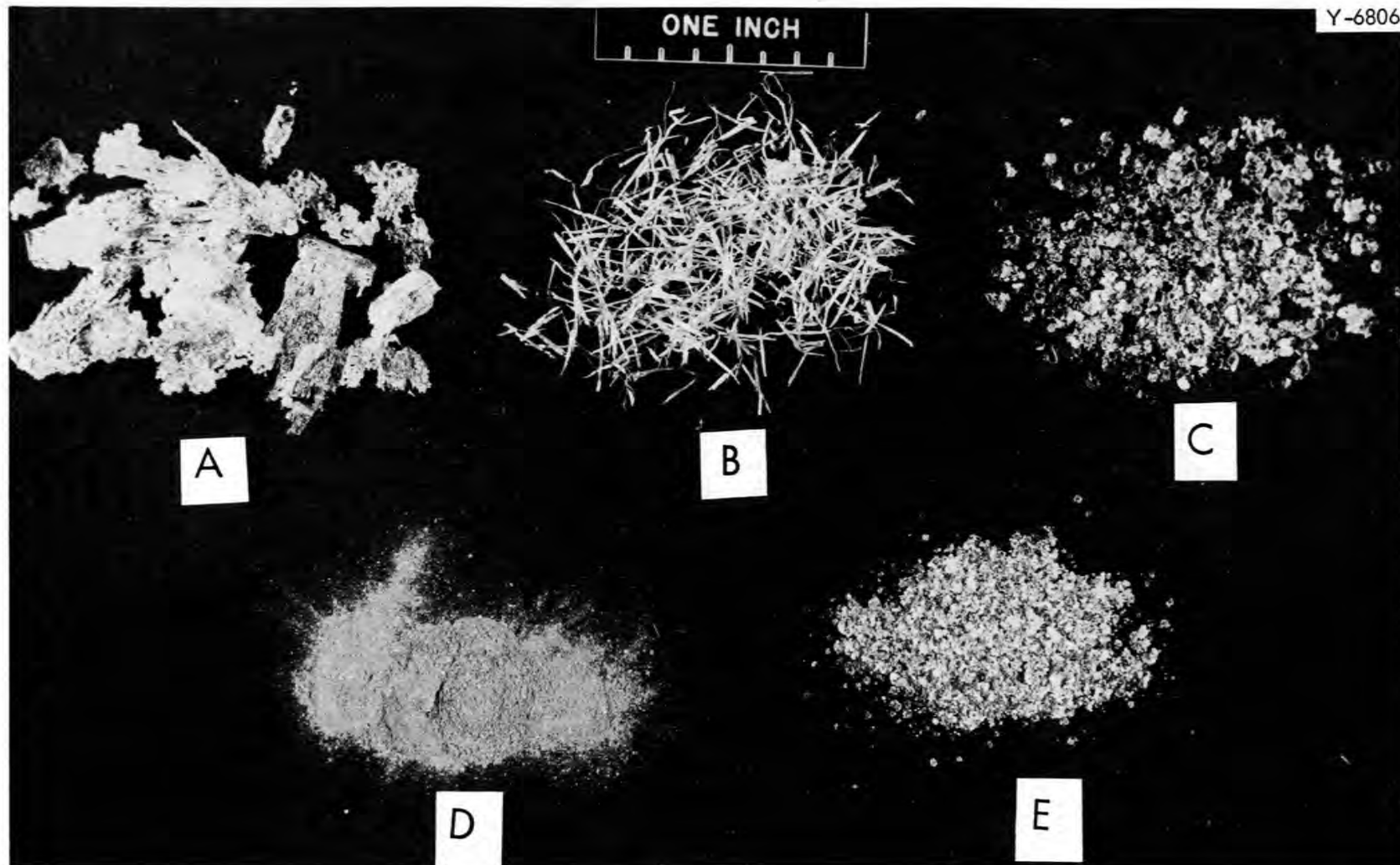


Fig. 1.2. Products of Three SLIS Processes for Alloy Powder Preparation Showing Effects of Ball Milling for 24 hr. (A) Prepared by horizontal-jet technique; (B) prepared by capillary-blown technique; (C) prepared by spinning-anode technique; (D) product A after ball milling; (E) product B after ball milling. Original reduced 13%.

Table 1.2. Hot Hardness of Thorium and Thorium-Base Alloys

Test Temperature (°C)	Hardness ^a (DPHN)							
	Arc-Cast		SLIS		Boronated			
	Th ^b	Th-5% Zr ^c	Th-1.3% Be ^d	Th-4.65% Zr ^e	Th-2.25% Zr ^f	Th-4.59% Zr ^g	Th-3.15% Zr ^h	
25	85	104	139	126	87	81	97	
100	45	93	140	i	i	i	i	
200	41	83	105	i	i	i	i	
300	35	90	105	i	i	i	i	
400	33	77	114	90	69	42	62	
500	30	71	86	69	59	39	60	
600	22	60	71	49	43	37	42	
700	15	42	45	40	27	29	23	
750	11	37	37	i	i	i	i	
800	i	i	28	28	15	20	10	

^aValues reported represent average of two measurements.

^bChemical analysis: Th, 99.8 wt %; C, 340 ppm; O, 2000 ppm; N, 180 ppm.

^cBased on arc-cast Th described in footnote (b).

^dPrepared by horizontal-jet SLIS method and hot-upset-extruded at 600°C.

^ePrepared from -325 mesh powders of dehydrided alloy powder and 1.1 wt % B, hot pressed at 1000°C and extruded at 750°C.

^fSame as described in footnote (e) except that blend contained 0.54 wt % B.

^gSame as described in footnote (e) except that -80 mesh powders of bomb-reduced alloy and 1.1 wt % B were used.

^hSame as described in footnote (e) except that -100 mesh powders of bomb-reduced alloy and 0.54 wt % B were used.

ⁱNot determined.

It is to be noted in Table 1.2 that between 600 and 750°C the Th-1.3 wt % Be SLIS alloy is somewhat harder than the Th-5 wt % Zr alloy. Metallographic studies revealed a tendency for the ThBe_{13} precipitate in the Th-1.3 wt % Be alloy to coarsen between 600 and 800°C. Figure 1.3 shows the microstructure of the Th-1.3 wt % Be alloy after extrusion at 600°C. Melting and SLISing of this alloy proved quite practicable. Impingement of the atomized particles against the quenching wheel was readily observable and easily controlled as a result of an incandescence of the molten thorium. Metallographic examination of the Th-1.3% Be powder revealed that the beryllium was retained completely in super-saturated solid solution.

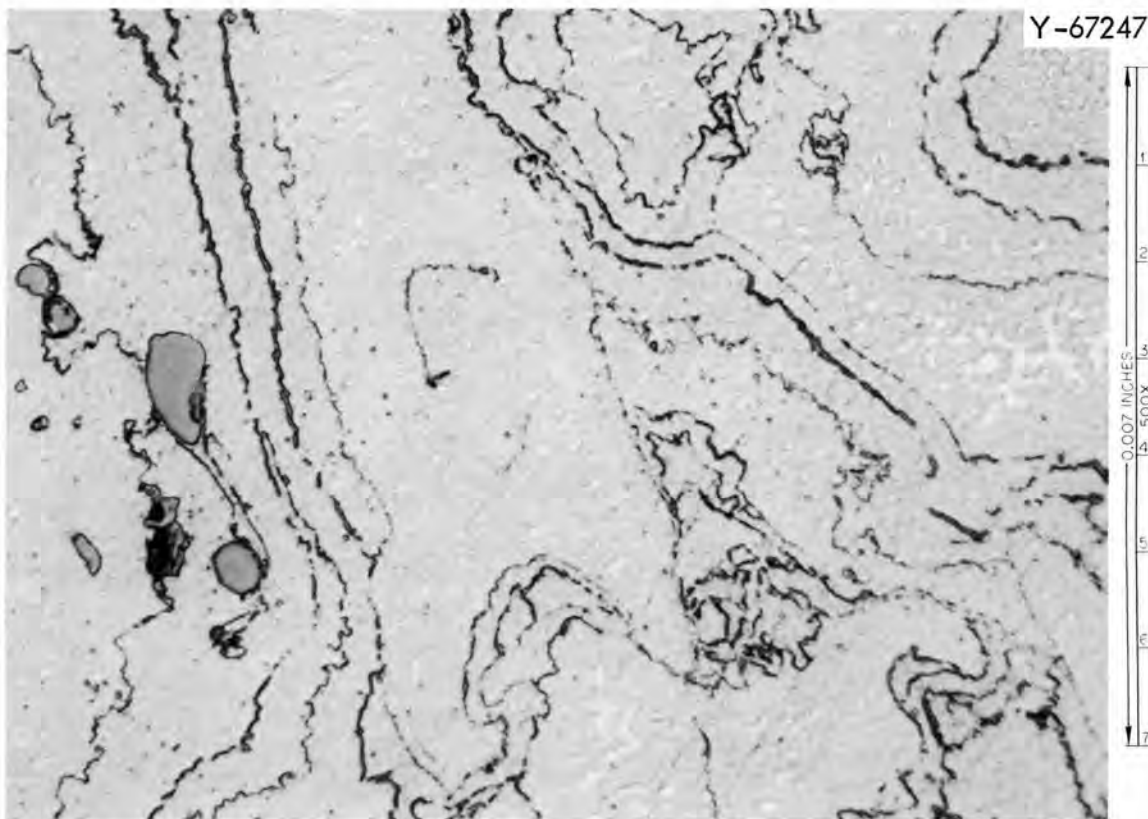


Fig. 1.3. Microstructure of the Th-1.3 wt % Be Alloy Prepared by the Horizontal-Jet SLIS Method and Upset-Extruded at 600°C. The massive dark gray constituents probably are ThO_2 inclusions introduced in the starting thorium melting stock; the fine jagged phase is ThO_2 formed on the surface of the SLIS powder; and the white phase is the precipitated ThBe_{13} compound. As-polished condition.

The hardness of the material dispersion hardened by boronating dehydrided Th-4.65 wt % Zr powder was comparable at 700 to 800°C to the Th-1.3 wt % Be SLIS alloy. Improvement in the boronated alloys is being sought by introducing the boron in a ball-milling operation and conducting the sintering at a lower temperature.

2. FUEL ELEMENT DEVELOPMENT

G. M. Adamson, Jr.

We have continued using thermochemical deposition as a means of fabricating refractory fuels and refractory metal cladding for high-temperature fuel elements. The fabrication behavior of UO_2 powders produced by direct reduction of UF_6 is being investigated using conventional cold-pressing and sintering techniques. Experiments in hydroreduction of uranium chlorides confirm that uranium dioxide may be produced either as a solid or a powder at high feed rates.

Experiments in reduction of UF_6 by lithium vapor have yielded uranium metal; however, engineering difficulties remain in metering lithium vapor. Ability to accurately meter the reactants of necessity precedes formation of refractory fuel compounds.

Experiments utilizing an external coating apparatus have reproduced homogeneous deposits of tungsten-rhenium tubing. A study of the deposit morphology in moving hot-zone internal deposits is continuing.

Deposition of Uranium Dioxide by Hydroreduction
of Uranium HexafluorideR. L. Heestand R. A. Potter¹ C. F. Leitten, Jr.

Studies of the fabrication characteristics of UO_2 powder produced by the hydroreduction of UF_6 were continued. The as-produced powder, which is high in fluorine (approx 5%) but shows no fluorine compounds on analysis, is hydrogen reduced at $1000^\circ C$ to give a low fluorine material.²

Figure 2.1 is representative of the as-produced powder at 165,000X by electron microscopy. Analysis of particle size indicated 99% of the

¹Ceramics Laboratory, Metals and Ceramics Division.

²R. L. Heestand and C. F. Leitten, Jr., Fuels and Materials Development Program Quart. Progr. Rept. Sept. 30, 1965, ORNL-TM-1270, pp. 9-10.



Fig. 2.1. As-Produced Uranium Dioxide Powder. Particle size 99% < 0.05 μ . 165,000X.

particles as being < 0.05 μ . When subsequently firing the material at 1000°C in moist hydrogen to remove fluorine and adjust the oxygen-to-uranium ratio, the powder size increases to give 99% of the particles < 9 μ as shown in Fig. 2.2 at 25,000X.

Sintering behavior of both materials is being investigated. Attempts to sinter as-produced powder have been negative due to breakup of the pellet by evolution of the fluorine apparently adsorbed on the powder.

Compacts of hydrogen fired powders were previously sintered at 1700°C to give a fine grain pellet having a density of 93% (ref. 2). To further investigate the behavior of this material, isotherms are being run to determine shrinkage and density as a function of firing time at temperature. It appears that initial sintering occurs at temperatures as low as 1300°C.

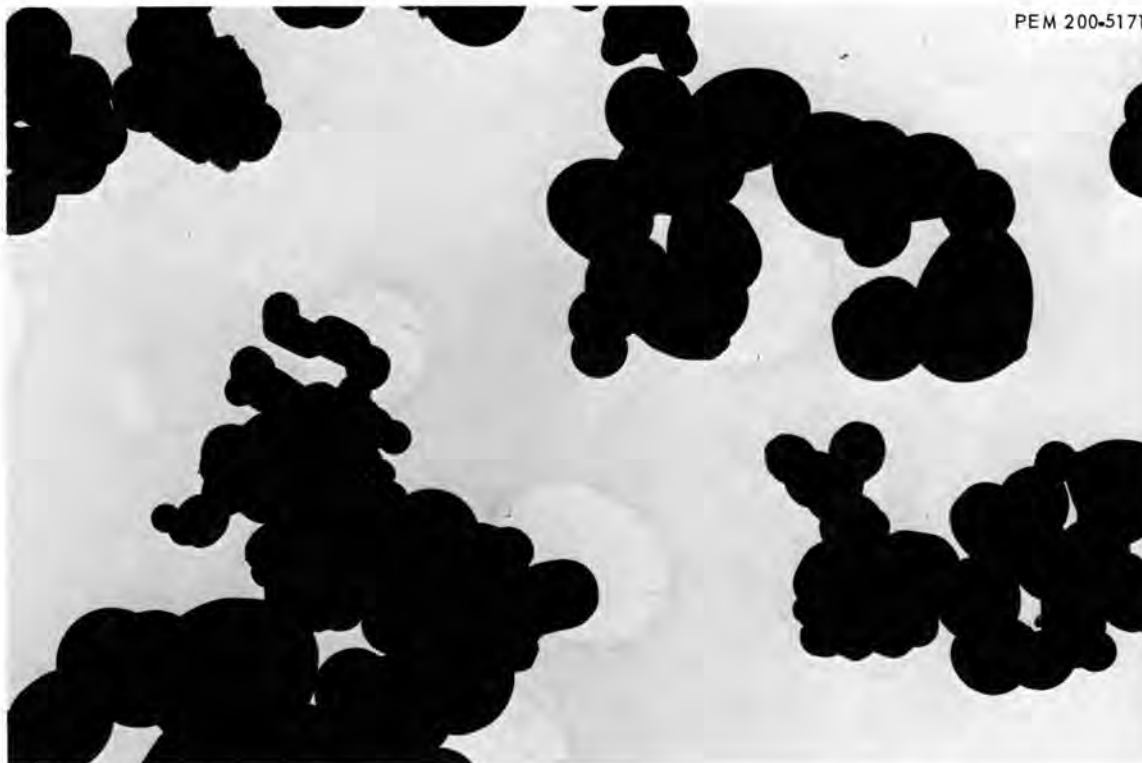


Fig. 2.2. Uranium Dioxide Powder Reduced 1 hr, 1000°C in Wet Hydrogen. Particle size 99% < 9 μ . 25,000X.

Deposition of Uranium Dioxide by Hydroreduction
of Uranium Tetrachloride

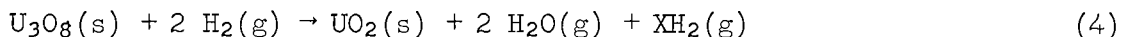
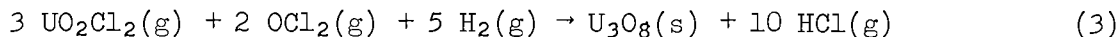
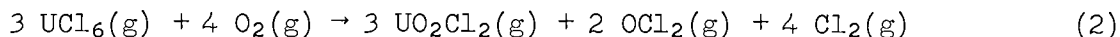
F. H. Patterson W. C. Robinson C. F. Leitten, Jr.

Reprocessing of spent Zircaloy-clad uranium oxide fuel elements yields the uranium as UCl_5 and UCl_6 (ref. 3). It has been demonstrated⁴ that these uranium chlorides can be reconstituted to UO_2 by an inexpensive thermochemical reaction that would be amenable to a "closed-loop" fuel recycle system. Small quantities of UO_2 were produced by the direct reaction of UCl_5 and UCl_6 with oxygen and the subsequent reduction of the intermediate reaction product by wet hydrogen.

³T. A. Gens, Chloride Volatility Experimental Studies: The Reaction of U_3O_8 with Carbon Tetrachloride and Mixtures of Carbon Tetrachloride and Chlorine, ORNL-TM-1258 (Aug. 26, 1965).

⁴F. H. Patterson, W. C. Robinson, Jr., and C. F. Leitten, Jr., Fuel and Materials Development Program Quart. Progr. Rept. Sept. 30, 1965, ORNL-TM-1270, pp. 10-11.

Additional experiments were run this quarter in an effort to optimize the deposition parameters. As before, "on stream" UCl_5 and UCl_6 were obtained by chlorinating uranium sheet at a temperature of 550°C and a pressure of 2 torr assuming the following sequence of reactions:



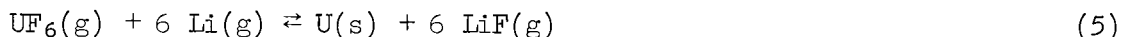
Reaction gas additives were made which more nearly approximated the stoichiometric relationships indicated in Eqs. (1), (2), and (3). While holding the reactor chamber at 850°C and 2 torr, Cl_2 , O_2 , and H_2 additives of 240, 192, and $720 \text{ cm}^3/\text{min}$ more than doubled the previous fuel yield. This material was subsequently reduced according to Eq. (4) to submicron-size powder having an oxygen-to-uranium ratio of 2.020.

Deposition of Uranium Compounds by Lithium Vapor
Reduction of Uranium Hexafluoride

W. C. Robinson

C. F. Leitten, Jr.

In the previous report,⁵ the feasibility of the reaction



was established, however, the reduction occurred at the point of UF_6 injection ultimately stopping the reaction. Equipment modifications were made in an attempt to transfer the reaction zone into the center of the

⁵W. C. Robinson, C. F. Leitten, Jr., Fuels and Materials Development Program Quart. Progr. Rept. Sept. 30, 1965, ORNL-TM-1270, pp. 10-12.

reaction chamber. Simultaneously, the separate lithium vaporization chamber was also discarded as being impractical since considerable difficulty had been encountered with condensation between the lithium chamber and the reaction chamber. The lithium was placed directly into the end of the reaction chamber in a small open stainless steel crucible. Difficulties were again encountered in attempting to form a flow of lithium vapor at or below temperatures of 1100°C. Since uranium metal melts at 1132°C, it is not desirable to operate above this temperature. Examination of the lithium metal after an attempted vaporization revealed a black film covering the entire surface of the metal. X-ray examination indicated that this film was Li_2C_2 and Li_3N with some LiF . Since the lithium is stored in kerosene, it was suspected that the organic had reacted with the lithium and prevented vaporization. An experiment was conducted in the absence of UF_6 which involved a 24-hr vacuum treatment of the metal at 0.05 torr at room temperature to remove hydrocarbon films prior to attempted vaporization. Using this technique, a very rapid flow of lithium vapor was established at temperatures of 750°C and above. This procedure was utilized in a subsequent UF_6 reduction experiment and a powder product was formed in the reaction zone. The product was identified by x-ray analysis as being a mixture of UO_2 , LiF , and very reactive uranium metal powder.

The UO_2 is believed to be formed when the product was washed with hot water for the purpose of facilitating removal of the inner liner of the reaction zone. The LiF remained in the reaction zone because 750°C is not sufficient to vaporize it.

These experiments establish that the product of the UF_6 -lithium reaction is a uranium powder under these conditions. A different product morphology may be realized at a lower lithium-to- UF_6 ratio. A method of controlling the flow of lithium vapor at higher temperatures rather than using excess lithium vapor is currently being studied.

Deposition of Tungsten Alloys

J. I. Federer

C. F. Leitten, Jr.

Previous codeposition experiments have utilized a moving hot zone for preparation of tungsten-rhenium alloys by hydrogen reduction of WF_6 and ReF_6 (ref. 6). Under the conditions of these experiments⁶ circumferential ridges form in the deposit on the inlet side of the hot zone (i.e., the region wherein deposition mainly occurs). The ridges subsequently grow in size upon passing through the hot zone giving an undesirable deposit. To investigate the cause of this behavior, several deposits were prepared by moving the deposition mandrel against the gas flow instead of with the gas flow, assuming that ridge growth would be minimized. This arrangement, however, caused peeling of the deposit from the mandrel resulting in a very rough surface. A possible explanation for this result is that successive layers of different composition formed at the outlet of the hot zone. Upon passing through the hot zone differences in thermal expansion among the layers caused separation of the deposit from the substrate. Unalloyed tungsten was deposited under similar conditions on stainless steel mandrels with no peeling, ridges, or other surface irregularities.

To investigate whether the ridges are associated with a reaction between the type 304 stainless steel mandrel and a rhenium halide, deposits were prepared in which the WF_6 -to- ReF_6 ratio was increased from 3:1 to about 17:1, the other conditions being held constant. In this case the deposit contained only a few shallow ridges with total recovery of rhenium and approximately 50% recovery of tungsten. Next an iron mandrel was used instead of stainless steel for a deposition under conditions that previously resulted in numerous ridges. This deposit had a smooth surface texture with only a few shallow ridges. These results indicate that reactions between the fluorides and the substrate can influence the deposition behavior.

⁶J. I. Federer, C. F. Leitten, Jr., Fuels and Materials Development Program Quart. Progr. Rept. Sept. 30, 1965, ORNL-TM-1270, pp. 12-17.

Thermodynamic calculations indicate that under equilibrium conditions the composition of the deposit will correspond to the metal content of the feed gases when the reduction occurs at about 1000°C. This result implies that deposits of uniform composition can be prepared in either a stationary or a moving hot zone. Experiments are now being conducted to test this hypothesis.

A tungsten-rhenium deposit of uniform composition was prepared in an external coating apparatus, previously described.⁶ During further experimentation the apparatus was modified to change the gas flow pattern in an effort to improve thickness uniformity of the deposits. The gases were made to enter the deposition chamber through a narrow annulus around the mandrel and exited through a similar annulus. The conditions and results of typical experiments are shown in Table 2.1. All experiments

Table 2.1. Condition and Results of Tungsten-Rhenium Codeposition Experiments in the External Coating Apparatus^a

Distance from Inlet (in.)	Rhenium Thickness							
	WRe-57		WRe-58 ^b		WRe-59 ^b		WRe-60 ^b	
	(%)	(mils)	(%)	(mils)	(%)	(mils)	(%)	(mils)
1	0.8		23.7		24.6	11.0	54.5	
2	1.4	16.2				13.1		7.5
3	1.9	19.3	1.4	13.0	1.1	14.4	29.4	10.0
4	2.4	20.8		12.0		14.4		12.1
5	3.3	20.0	0.2	11.0	0.2	13.5	8.2	13.0
6	2.8	17.9		9.8		11.8		12.1
7	4.1	13.4	0.04	8.5	0.4	10.0	1.1	10.0
8	2.3	9.6		7.5		8.3		8.6
9	1.7		0.03		0.2	6.5	0.1	7.5
10	1.1					5.0		6.7
11			0.02		0.2		0.1	

^aTest conditions: Temperature, 600°C; pressure, 10 torr; hydrogen, 1000 cm³/min; WF₆, 95 cm³/min except WRe-60, 90 cm³/min; ReF₆, 5 cm³/min except WRe-60, 10 cm³/min.

^bApparatus modified, see text.

except WRe-57 were performed in the modified apparatus. The data show that the modification had no substantial effect on thickness uniformity but had an adverse effect on composition uniformity resulting in a high rhenium content near the inlet.

Rhenium-rich deposits also were prepared in the modified apparatus. These deposits were characterized by a thin, smooth coating near the inlet and an abrupt change to a thick, nodular deposit at the middle.

Deposition of Molybdenum

J. I. Federer

C. F. Leitten, Jr.

Previous attempts to deposit molybdenum by hydrogen reduction of MoF_6 have been hampered by an inadequate metering system for MoF_6 . Recent installation of a mass flowmeter⁷ has allowed deposition experiments to continue in a systematic manner. The conditions and results of these experiments are shown in Table 2.2. The recovery data appears to be anomalous in that recoveries apparently increase with decreasing temperature. The reduction of MoF_6 by hydrogen, however, involves a slow reduction step in which an intermediate halide, MoF_3 , is formed. The proportion of MoF_3 deposited along with metal increases with decreasing temperature resulting in misleading recovery values. Presently, higher temperatures are preferred for molybdenum deposition, and future experiments will utilize a moving hot zone in an effort to deposit long, uniform tubes.

⁷Hastings Raydist, Inc., Hampton, Virginia.

Table 2.2. Conditions and Results of Molybdenum Deposition Experiments

Temperature ^a (°C)	Pressure (torr)	Hydrogen ^b (cm ³ /min)	MoF ₆ (cm ³ /min)	Recovery (%)	Description of Deposit
800	10	2000	45	84	Dark rough coating near the inlet followed by a smooth metallic coating.
800	10	2000	45	78	Thin dark coating near the inlet followed by a smooth metallic coating having a maximum thickness of about 30 mils.
700	10	1000	25	92	Thin dark coating near the inlet, becoming more metallic with increasing distance. Metallic whiskers 4 in. from the inlet. Dark coating further downstream.
700	10	1000	45	100	Similar to 700°C deposit above.
600	10	1000	45	95	Dark colored coating with irregular growths near the inlet. Thin metallic coating further downstream.

^aStationary hot zone: 12 in. long.

^bMetering pressure: 550 torr.

3. MECHANICAL PROPERTIES

J. R. Weir, Jr.

One objective of this program is to determine the effect of irradiation on the mechanical properties of alloys of interest as fuel cladding and to find a metallurgical condition for the alloys that produces the least effect of subsequent irradiation on the mechanical properties. To accomplish this, our study concerns the interaction of radiation-induced defects and the substructure of the alloys, the effect of irradiation temperature, postirradiation test variables, and neutron dosimetry in the facilities used in the irradiations. The material selected for initial study is type 304 stainless steel.

Irradiation Embrittlement in Titanium-Bearing
Type 304 Stainless Steel

W. R. Martin

E. E. Bloom

Investigation of the resistance of the type 304 stainless steel plus 0.2 wt % Ti alloy to elevated-temperature irradiation embrittlement is continuing. The complete results of the low- and high-carbon alloys are given in Table 3.1. Recent results on the alloy irradiated at 700°C for 2000 hr are given in Table 3.2, and type 304 stainless steel data are shown also for comparison. Although the ductility of the titanium-bearing alloy has been reduced when irradiated to the higher dose, the ductility of the 0.2 wt % Ti alloy is substantially better than regular type 304 stainless steel.

We are engaged in both fractographic and transmission micrographic examination of these alloys in order to better study the irradiation embrittlement. Our fractographic studies have just begun; therefore it is too early to ascertain the significant differences in behavior of irradiated and unirradiated alloys.

The specimens irradiated to a dose level of 1×10^{20} neutrons/cm² (thermal) and 1.5×10^{19} neutrons/cm² ($E > 1$ Mev) have been examined for helium bubbles. No bubbles are observed in the as-irradiated condition (50°C) for either the regular type 304 stainless steel or the

Table 3.1. Influence of Titanium on the Elevated-Temperature Irradiation Embrittlement of 18-8 Stainless Steel^a

Titanium (wt %)	Total Elongation ^b (%) ^c					
	0.02 wt % C Alloy at:			0.06 wt % C Alloy at:		
	700°C		842°C	700°C		842°C
0.0	21.6	(36.0)	13.1 ^d (45.8)	31.5	(35.4)	20.0 (44.0)
0.2	35.2	(40.9)	60.4 ^d (71.3)	38.0	(32.6)	45.1 (47.2)
0.3	26.0		33.9 (53.3)	28.5	(25.5)	35.2 (43.6)
0.4	25.9	(30.2)	18.9 (40.3)	26.5	(28.3)	25.0 (42.7)
0.5	25.1	(29.8)		21.5	(25.3)	19.0 (35.4)
0.6	23.3	(31.9)	14.8 (35.3)	19.5	(24.0)	17.9 (37.4)
0.8	26.5	(34.8)	13.1 (33.6)	20.5		19.1
1.0	26.1	(52.4)	12.3 (45.9)	23.5		23.5
1.2		(57.1)	11.5 (46.0)	23.0		28.5 (68.0)

^aSpecimens irradiated to a dose level of 1×10^{20} neutrons/cm² (thermal) and 1.5×10^{19} neutrons/cm² ($E > 1$ Mev).

^bMeasured in a 1-in. gage length for tests at a strain rate of 2%/min.

^cNumbers in parentheses represent ductility values of unirradiated material.

^dSamples taken from these alloys for transmission microscopy studies.

Table 3.2. Ductility of Stainless Steels After Irradiation at 700°C^a

Deformation Temperature (°C)	Ductility (% Total Elongation)			
	Regular Type 304 Stainless Steel		0.2 wt % Ti Alloy	
	Unirradiated	Irradiated	Unirradiated	Irradiated
704	39	11	48	18
842	47	4	74	23

^aThe 0.02 wt % C alloys were irradiated for 2000 hr to a dose level of 9×10^{20} neutrons/cm² (thermal) and 7×10^{20} neutrons/cm² (fast) and tensile tested at a strain rate of 0.2%/min.

0.2 wt % Ti-bearing type 304 stainless steel alloy. Bubbles can be found in the grain boundaries of the type 304 stainless steel after a postirradiation anneal of 1 hr at 1100°C, using the electron microscope as a detection device. However, no bubbles were found in the titanium-bearing alloy even after a postirradiation anneal of 1 hr at 1260°C.

A comparison of the transmission micrographs of both alloys reveals other significant differences. The type 304 stainless steel is mainly devoid of precipitate while the titanium-bearing alloy contains both inter- and intragranular precipitate. Our earlier hypothesis for the improved ductility observed in the titanium alloy was based on forming helium from the (n, α) reactions at the precipitate matrix interface within the grains. Certainly the micrographs confirm that we have removed the helium from the grain boundaries but convincing evidence for helium at the precipitates is lacking.

Our examination of helium behavior in the titanium-bearing and regular type 304 stainless steel will continue and include the steels containing higher titanium levels.

Mechanical Properties of Titanium-Modified Type 304 Stainless Steel

E. E. Bloom

An investigation has been initiated to determine the effects of heat treatment, aging of elevated temperature, and composition on the short-time tensile and creep-rupture properties of the titanium-bearing alloy.

Two commercial heats of the titanium-modified type 304 stainless steel have been obtained and are being compared to a normal type 304L stainless steel. The two heats are very similar except for carbon content. Heat D-6 contains 0.053 wt % C and heat D-9 contains 0.014 wt % C. The chemical analyses of the three steels are given in Table 3.3.

In the as-received condition the three alloys were in the form of 1/2-in.-diam rod. These were swaged to 3/8-in. diameter, annealed for 1 hr at 1036°C and swaged to 1/4-in.-diam rod. Subsize tensile and creep

Table 3.3. Composition of Experimental Materials

Heat Number	Element, wt %									
	C	S	Mn	Si	Cr	Mo	Ti	Cu	Ni	P
Type 304 stain- less steel heat 33107	0.057	0.016	0.76	0.48	19.0				8.92	0.02
D-6	0.053	0.004	1.53	0.7	19.0	<0.05	0.15	0.07	0.34	0.006
D-9	0.014	0.005	1.54	0.72	18.31	<0.03	0.14	<0.03	10.04	0.005

specimens with 1/8-in.-diam and 1-in.-long gage dimensions were machined from this rod.

The effect of solution annealing temperature upon short-time tensile properties has been determined. Specimens were annealed for 1 hr at 1036, 1177, and 1260°C and cooled in the cold zone of the furnace, which is slightly faster than air cooling. Tensile tests were run on a 10,000-lb-capacity Instron using a crosshead speed of 0.02 in./min and five testing temperatures. Results are summarized in Table 3.4.

Yield stress and ultimate tensile strength data indicate that the effect of increasing the solution annealing temperature is to decrease the strength. Although metallographic studies have not been completed, it is reasonable to assume that this is due to the larger grain sizes resulting from higher solution annealing temperatures. As the testing temperature is increased to 650°C and above, the effect of solution annealing temperature upon yield stress and ultimate tensile strength becomes negligible in short-time tensile tests.

Although strength values are nearly the same in each of the three alloys the ductility values are not. Regular type 304 stainless steel, solution annealed at 1036°C, drops from 84% elongation at room temperature to 36% elongation at 538°C and remains between 30 and 36% up to 870°C. Both heats of titanium-modified type 304 stainless steel, annealed at 1036°C, exhibit a similar drop in elongation between room temperature and 538°C; however ductility is regained as the testing temperature is increased. At 871°C elongation values between 59% (heat D-9) and 77% (heat D-6) were obtained.

The effect of solution annealing temperature on elevated-temperature ductility is significant. Heat D-6, which contains 0.053 wt % C, has slightly better ductility when annealed at 1177°C rather than 1036°C. However, elevated-temperature ductility decreases when the annealing temperature is increased to 1260°C. Heat D-9, which contains 0.014 wt % C, exhibits its best elevated-temperature ductility when annealed at 1036°C.

Tests are being carried out to determine the creep-rupture properties of both heats of titanium-modified stainless steel and the one heat of regular type 304L stainless steel at 593, 705, and 815°C.

Table 3.4. Effect of Solution Annealing Temperature on the Tensile Properties of Type 304 Stainless Steel and Type 304 Titanium-Modified Stainless Steel

Material	Testing Temperature (°C)	Solution Annealed at 1036°C			Solution Annealed at 1177°C			Solution Annealed at 1260°C		
		Yield Stress (1000 psi)	Ultimate Tensile Strength (1000 psi)	Total Elongation (%)	Yield Stress (1000 psi)	Ultimate Tensile Strength (1000 psi)	Total Elongation (%)	Yield Stress (1000 psi)	Ultimate Tensile Strength (1000 psi)	Total Elongation (%)
Type 304 stainless steel, heat 33107	Room temperature	31.98	93.33	84.2						
	538	14.75	63.77	36.0						
	649	13.88	43.80	29.1						
	760	12.40	27.11	36.2						
	871	10.66	13.52	32.0						
Type 304 stainless steel, titanium moderated, heat D-6	Room temperature	23.14	90.74	83.7	22.08	89.67	94.0	20.07	82.64	86.8
	538	11.57	59.83	39.7	9.66	56.30	41.4	5.52	52.85	44.6
	649	11.57	43.77	40.8	8.82	41.18	41.6	7.92	40.00	37.4
	760	9.92	22.48	63.1	9.09	21.49	65.5	7.85	21.48	39.8
	871	9.09	12.23	77.4	10.67	13.03	80.9	10.41	12.33	55.8
Type 304 stainless steel, titanium moderated, heat D-9	Room temperature	21.42	92.94	78.1	19.83	87.75	83.4	19.66	83.63	75.8
	538	11.34	54.87	35.9	6.41	49.15	35.2	6.78	51.69	33.3
	649	9.24	37.82	47.5	7.56	37.82	41.6	6.78	37.77	30.1
	760	8.40	19.38	65.3	6.97	22.26	55.6	8.66	24.12	34.0
	871	8.40	13.03	59.2	7.50	11.50	58.9	7.98	10.84	40.2

At present the results are incomplete and the only comparison that can be made is between regular type 304 stainless steel and one heat (heat D-6) of the titanium-modified stainless steel at 815°C. For these conditions the titanium-modified steel has slightly better creep and rupture strength at lower stresses as seen in Table 3.5. Also, ductility values are considerably better in the titanium-modified steel.

Table 3.5. Creep Properties of Type 304L and Titanium-Modified Type 304 Stainless Steel at 815°C

Material	Initial Stress (psi)	Rupture Life (hr)	Minimum Creep Rate (%/hr)	Total Elongation (%)
Type 304 stainless steel, heat 33107	14,000	1.45	20.4	49.0
	12,000	4.6	4.8	42.7
	10,000	16.9	1.2	32.1
	8,000	25.9	0.84	28.5
	7,500	95.0	0.28	29.7
	5,000	735.0	0.0145	18.1
Type 304 stainless steel, titanium modified, heat D-6	18,000	0.31	138.0	80.3
	15,000	1.35	36.5	93.7
	12,000	8.9	5.75	72.0
	9,000	60.0	0.575	81.3
	7,500	248.0	0.072	51.3

Postirradiation Creep and Stress-Rupture of
Type 304 Stainless Steel

W. R. Martin

The postirradiation evaluation of type 304 stainless steel in short-time tensile tests has revealed many metallurgical treatments that result in a more ductile irradiated steel. Since the ductility of irradiated steels is very sensitive to strain rate, we are also evaluating these heat treatments, using postirradiation stress-rupture tests.

Our initial tests are at 650°C in air and the second series will be tested at 815°C. The current information on the 650°C set is given in Table 3.6. The tests completed to date again show that a fine grain size is preferred over the coarse grain material. The ductility and

Table 3.6. Postirradiation Creep of Type 304 Stainless Steel at 650°C

Stress (1000 psi)	Time to Rupture, hr ^a			Total Elongation, ^a %		
	Pretreatment			Pretreatment		
	A	B	C	A	B	C
30	11.3	1.5	14.8	44.0	11.4	24.2
25	79.0	5.5	50.8	29.5	9.0	25.0
20	b	109.5	c		4.8	
15	c	194.4	b		8.9	

^aA denotes 1-hr anneal at 900°C in argon (ASTM 9).

B denotes 1-hr anneal at 1036°C in argon (ASTM 5).

C denotes 1-hr anneal at 1036°C + 100 hr at 800°C (ASTM 5).

^bScheduled.

^cIn progress.

time to rupture is substantially improved. The aging treatment given the coarse grain size material improved the ductility and rupture life. The improved ductilities by aging and refining the grain size are the same as noted previously,¹ using short-time tensile tests.

Several factors which could result in the improved ductility, such as the influence of reduced grain size and agglomerated grain-boundary carbides, were discussed earlier. An additional mechanism by which the agglomerated carbides may influence the stress-rupture test is one noted by Garofalo.² A short aging treatment of 24 hr at 816°C after solution anneal improves the rupture life and ductility of stainless steel tested at 593°C. The fracture behavior of the alloy was not changed, but the effect of the aging treatment was attributed to grain-boundary migration. The migration of boundaries between the spheroidized precipitate delayed the intergranular fracture. We have not noted the grain-boundary migration to any larger degree in our short-time tensile tests. Metallographic examination of the stress-rupture specimen will be conducted in the next reporting period.

¹W. R. Martin and J. R. Weir, "Irradiation Effects in Stainless Steels at Elevated Temperatures," p. 36 in Proceedings of Sodium Components Development Information Meeting, AEC Report CONF 650620 (1965).

²F. Garofalo, Fundamentals of Creep and Creep-Rupture in Metals, p. 223, The Macmillan Com [redacted] 5.

Elevated-Temperature Embrittlement of Structural
Material Welds and Brazes

W. R. Martin

The effect of irradiation on the elevated temperature ductility and ultimate strength of welds and brazes are being studied. We have chosen to study first the properties of type 304 stainless steel and Inconel 600 as they represent materials that have been used extensively in reactor construction. Tensile specimens have been machined from the base metal, weldment and joint area for both type 304 stainless steel and Inconel 600 welded plate. Both alloys were brazed with the brazing alloy AWS-BNi7 and are being evaluated, using a subsized Miller-Peaslee specimen. All specimens were irradiated in the as-welded or as-brazed condition.

The specimens were irradiated in a poolside position of the Oak Ridge Research Reactor at approximately 50°C to a neutron dose of 6.7×10^{19} neutrons/cm² (thermal) and 2.3×10^{18} neutrons/cm² ($E > 1$ Mev). The type 304 stainless steel specimens have been tested and the results are given in Tables 3.7 and 3.8.

The data on the type 304 stainless steel welds are consistent with previous data on type 304 stainless steel materials. The reduction in ductility observed for deformation temperatures above 500°C is not accompanied by increases in strength. The base metal, weldments, and joint specimens behaved in a similar fashion. These welds were prepared with a heat of type 308L stainless steel welding rod which contained approximately 75 ppm B. This is unusually high for the 300 series stainless steels. The base metal contained 6.8 ppm B, while the actual weld metal contained approximately 50 ppm B. A greater effect of irradiation was noted on the welds than for the base metal but was not as large a difference as was anticipated. Very likely the cast structure of the weld is influencing the embrittlement. Postirradiation metallography may reveal some important factors. Finally, in the irradiated condition all joints failed in the base-metal or heat-affected zone, except for the joint tested at 600°C which failed in the weld metal. It appears to be the same for the irradiated materials; however, metallographic samples to be processed shortly will confirm the location of the fracture.

Table 3.7. Ductility of Irradiated and Unirradiated Type 304
Stainless Steel Welds

Deformation Temperature (°C)	Location from Which Specimen Was Machined			Total Elongation at Fracture, %	
	Base Alloy	Weld Metal	Joint Heat- Affected Zone and Weld Metal	Unirradiated Condition	Irradiated Condition
Room	x	x		89.9	72.4
100	x		x	27.9	47.6
200	x		x	28.1	21.6
300	x		x	22.2	16.5
400	x		x	20.0	12.9
500	x		x	20.6	12.9
600	x		x	25.1	13.4
700	x		x	41.1	40.0
800	x		x	25.0	21.3
900	x		x	25.5	19.2
				39.4	38.0
				21.1	23.8
				21.6	23.1
				37.8	23.2
				27.1	13.4
					12.1
				21.5	9.5
				31.4	12.8
				15.8	5.7
				20.2	4.9
				30.2	4.1
				17.3	

Table 3.8. Effect of Irradiation on the Load-Carrying Ability of
Type 304 Stainless Steel - AWS-BNi7 Brazes*

Shearing Temperature (°C)	Joint Load-Carrying Capacity in Tensile Shear (lb per 1/8 in. of linear joint)		Effect of Irradiation		
	Unirradiated	Irradiated	Increased Load	Decreased Load	Change (%)
Room	518	665	x		28
100	430	620	x		44
200	407	540	x		33
300	377	470	x		25
400	358	464	x		26
500	366	387	x		6
600	380	368		x	3
700	357	290		x	19
800	246	228		x	7
900		108			

The maximum load supported by the Miller-Peaslee specimen was influenced by irradiation. For shear tests below 500°C the load was increased. Above 500°C the maximum load was decreased. The effect of irradiation above 500°C is greater than that indicated by these maximum load values. If one compares the load-extension curves of irradiated and unirradiated specimens, a very large decrease in the ductility of the specimens is noted, particularly at 800°C. We hesitate however to quote values for ductility because of the apparent deformation in the base alloy.

These type tests on welds and brazes should continue. The effects of grain refinement on the base metal, welding rod with a lower boron content, and preirradiation heat treatments of weldments need to be examined for type 304 stainless steel and type 304 stainless steel containing titanium.

4. NONDESTRUCTIVE TEST DEVELOPMENT

R. W. McClung

Our program is intended to develop new and improved methods of evaluating reactor materials and components. To achieve this we have studied various physical phenomena, developed instrumentation and other equipment, devised application techniques, and designed and fabricated reference standards. Among the methods being actively pursued are electromagnetics (with major emphasis on eddy currents), ultrasonics, and penetrating radiation. In addition to our programs oriented toward the development of methods, we are studying these and other methods for evaluation of problem materials and developing techniques for remote inspection.

Electromagnetic Test Methods

C. V. Dodd

Analytical Studies

We have continued research and development on electromagnetic phenomena on both an analytical and empirical basis. As part of our program we are studying the mathematical determination of electromagnetic phenomena of a coil as a function of coil dimensions, frequency, specimen conductivity and permeability and coil-to-specimen spacing. Most recently we have investigated the forces produced by eddy currents. The eddy-current forces produced on the interior of the conducting specimen can be resolved into an alternating force and a steady force. The axial component of this steady force was both measured and calculated for a coil in a ferrite cup above a conducting ring, as shown in Fig. 4.1. The calculated and normalized contours of the force density inside the ring are also shown in the figure. The calculated values of the net force was 0.5 to 17% greater than those we measured. However, the value of the permeability used in the calculations was 17% higher than the permeability of the ferrite cup used, which would give this type of error.

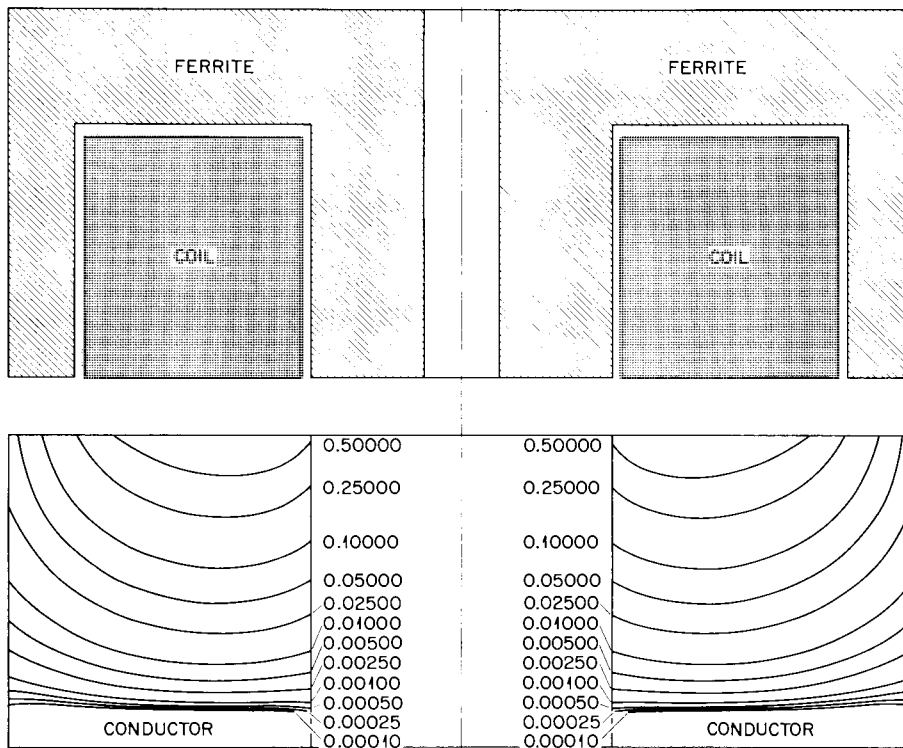


Fig. 4.1. Determination of Axial Eddy-Current Forces in a Conducting Ring.

These calculations can be used to study the noncontact generation of ultrasonic pulses by eddy currents, as well as being applicable to many other areas of technology, such as magna-forming, induction pumping, and magnetohydrodynamic generation of electricity.

Phase-Sensitive Eddy-Current Instrument

Improvements have been made recently on the stability of the phase-sensitive eddy-current instrument. The instrument now has less than 0.2° phase shift for a 20°C temperature change.

Ultrasonic Test Methods

K. V. Cook

Nonbond Studies

We have continued our studies on the behavior of ultrasound in thin sections with the principal effort being the detection of nonbonds in

cladding structures. We have been developing¹ a system for the evaluation of fuel tubes for nonbonding and have now successfully adapted the method to remote operation and used it in a hot (radiation level) laboratory.

The mechanical system for helically scanning fuel tubes is shown in Fig. 4.2. In actual operation the motor-driven scanning device (on the right) is inside the cell. The control and recorder which are outside the cell are shown on the left.

¹K. V. Cook, Fuels and Materials Development Program Quart. Progr. Rept. June 30, 1965, ORNL-TM-1200, p. 27.

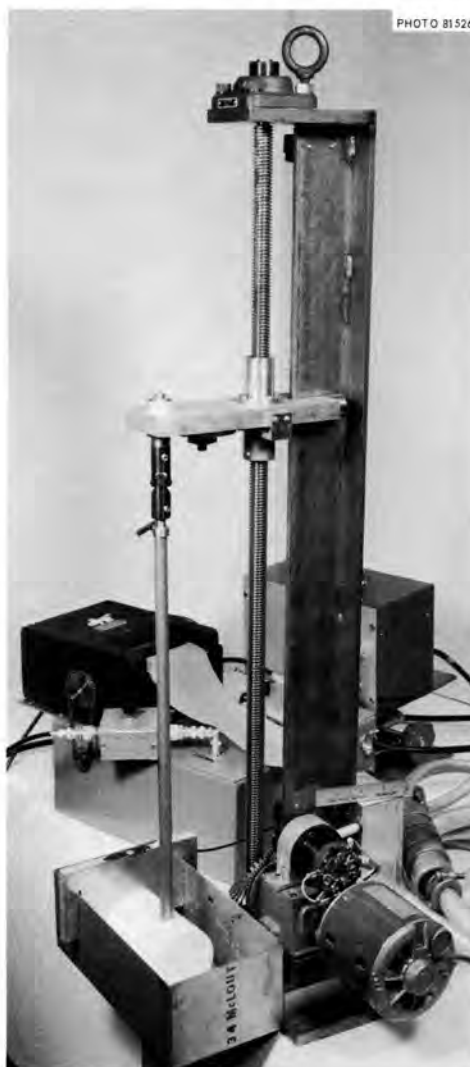


Fig. 4.2. Mechanical System for Helically Scanning Fuel Tubes in a Hot Cell.

Tubing Inspection

We are continuing to work on the problems encountered in tubing inspection. A major problem is the establishment of realistic reference notch standards for calibration. Electrical-discharge machining appears to be a reliable method for making both inner- and outer-surface notches, and we are continuing to use this technique for our studies. Previously, all our work has been on machining of longitudinal notches; however, we are now studying the problems associated with fabricating circumferential notches on both the inside and the outside of tubing. Calibration of the equipment is more complex for the circumferential notches than for the longitudinal. For instance, we have found that to get an 0.003-in.-deep $\pm 10\%$ notch in a tube that has an outside diameter of 0.420 in., we must preshape the tool to an outer diameter of approximately 0.339 in. If the tool is originally shaped to fit the outer diameter of the tube itself (0.420 in.), the center of the fabricated notch will be considerably deeper than the outer edges. As is evident, each time a notch is fabricated the tool must be reshaped and thus the process is much more time consuming than for longitudinal notches.

Schlieren System

We have assembled a Schlieren system for viewing and photographing ultrasound as it travels in a transparent medium. We can view continuous-wave beams emerging from the transducer face as is shown in Fig. 4.3 and can also view pulsed-ultrasonic packets of sound by using a short duration light flash (0.2 μ sec).

The system is shown in Fig. 4.4 along with the ultrasonic oscillator and transducer assembly. The triangular base is an optical bench and is used to align the required components for the ultrasonic photography system.

We plan to use this versatile and sensitive Schlieren system to study beam shapes coming from different types and frequencies of transducers as well as to monitor reflections and refractions of these beams and wave packets from interfaces. We also plan to use the system to study Lamb wave and other ultrasonic phenomena.

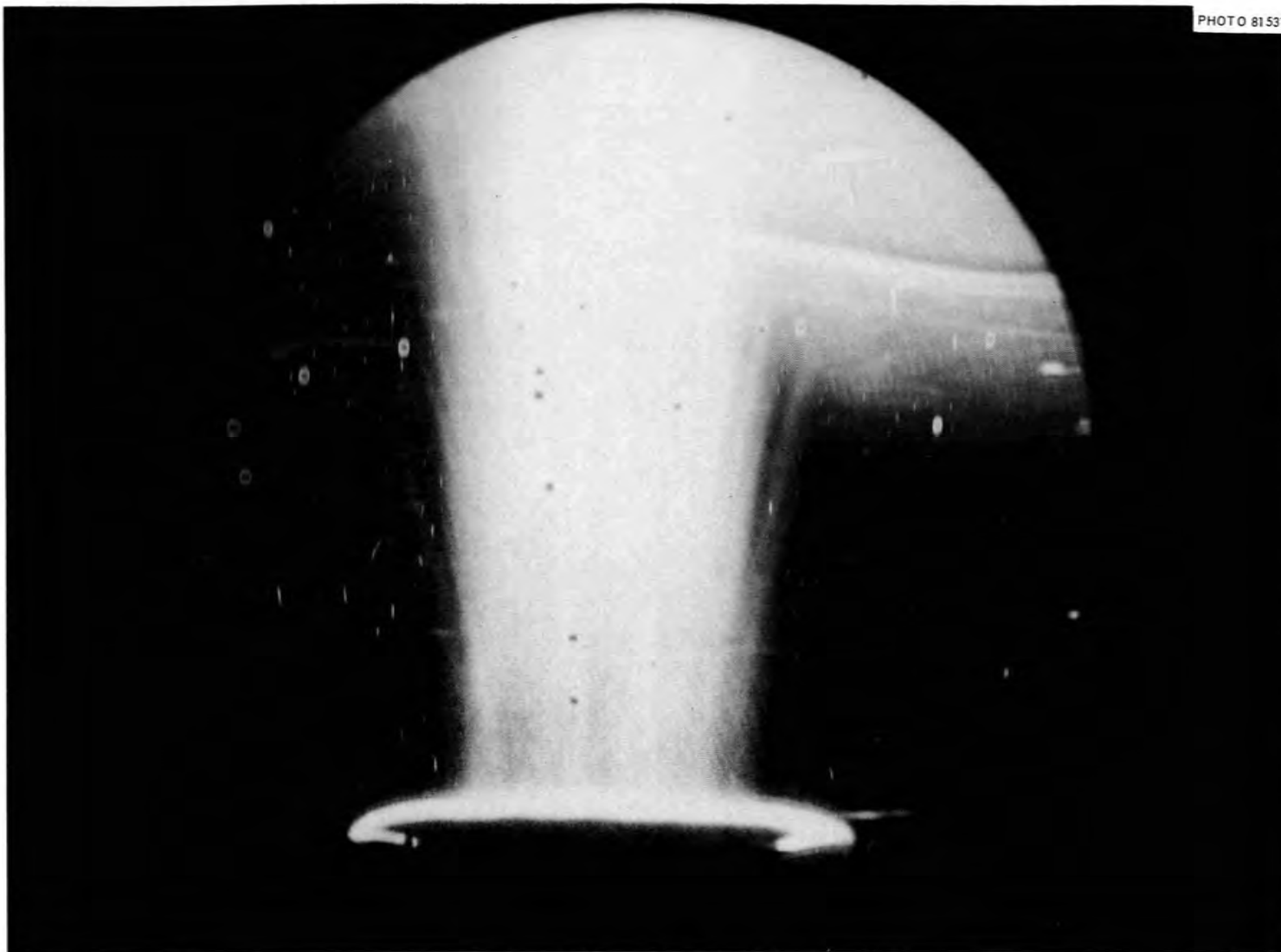


Fig. 4.3. Continuous-Wave Ultrasonic Beam as Seen With a Schlieren System.

OFFICIAL USE ONLY

OFFICIAL USE ONLY

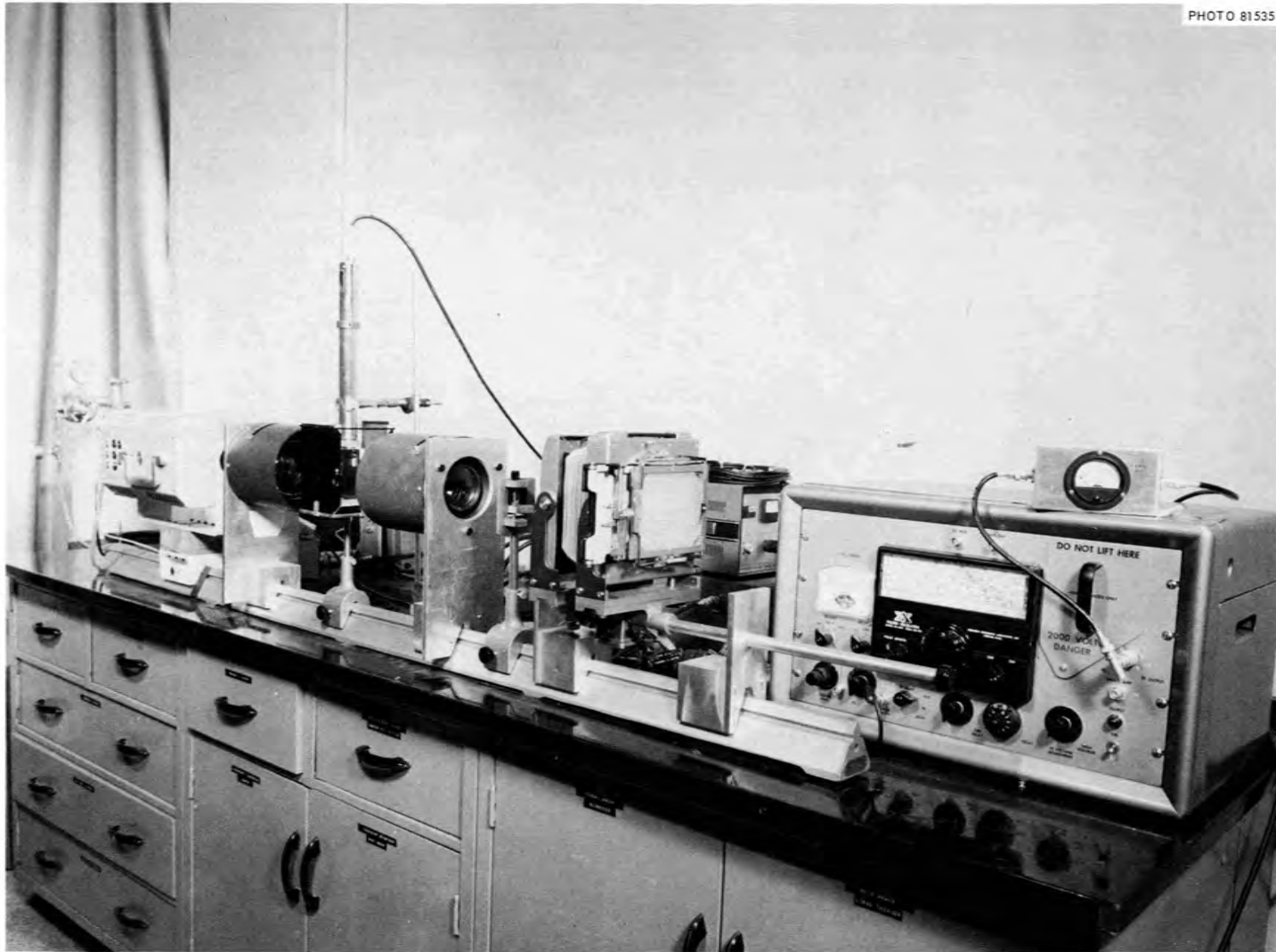


Fig. 4.4. Schlieren System for Viewing Ultrasound.

Penetrating Radiation

X- and Gamma-Ray Attenuation Gaging - B. E. Foster, S. D. Snyder

Fuel Element Homogeneity - We are continuing the study of x- and gamma-ray attenuation for the evaluation of fuel elements. Variation in transmitted intensity is monitored readily using a scintillation detector and is then related through proper calibration to the fuel loading homogeneity within the area of interest. We have completed the data analysis on the two vibratorily-compacted, 1/2-in.-diam (Th-3 wt % UO₂) fuel rods, six 1/2-in.-diam ThO₂ pellets, and eight 3/4-in.-diam ThO₂ pellets. These samples were scanned at longitudinal speeds of 2, 4, 8, 12, 16, 20, and 24 in./min using collimation of 1/8 × 1/8 in. and 1/8 × 1/2 in. with ⁶⁰Co and ¹³⁷Cs as the radiation sources. A series of graphs was constructed plotting radiation attenuation (chart reading) vs longitudinal scan speed and specimen thickness-density product for both types of collimation, both sources and all speeds. Figure 4.5 shows typical data for the use of ⁶⁰Co.

We define the calibration of the system as the average instrumentation response to a given change in fuel concentration. This should not be confused with resolution that defines the size of the smallest detectable inhomogeneity. When ⁶⁰Co was used as the radiation source, the average response remained essentially constant for both size rods and both collimator sizes at scan speeds of 2 through 24 in./min.

The same parameters were varied using ¹³⁷Cs as the radiation source. The average response remained constant for the 1/2-in.-diam rods, but there was a shift in calibration on the 3/4-in.-diam rods. This indicates that the radiation energy of ¹³⁷Cs is too soft for efficient homogeneity evaluation on 3/4-in.-diam rods.

In addition, the scan traces indicate some degree of smoothing of the small spot inhomogeneities with the use of larger collimation. This is not an improvement in spot homogeneity, but merely an averaging or smoothing over a larger area.

We are further evaluating the system for fuel-rod homogeneity measurements by determining the effect on calibration when there is a change in the wall thickness of the tube that houses the fuel material.

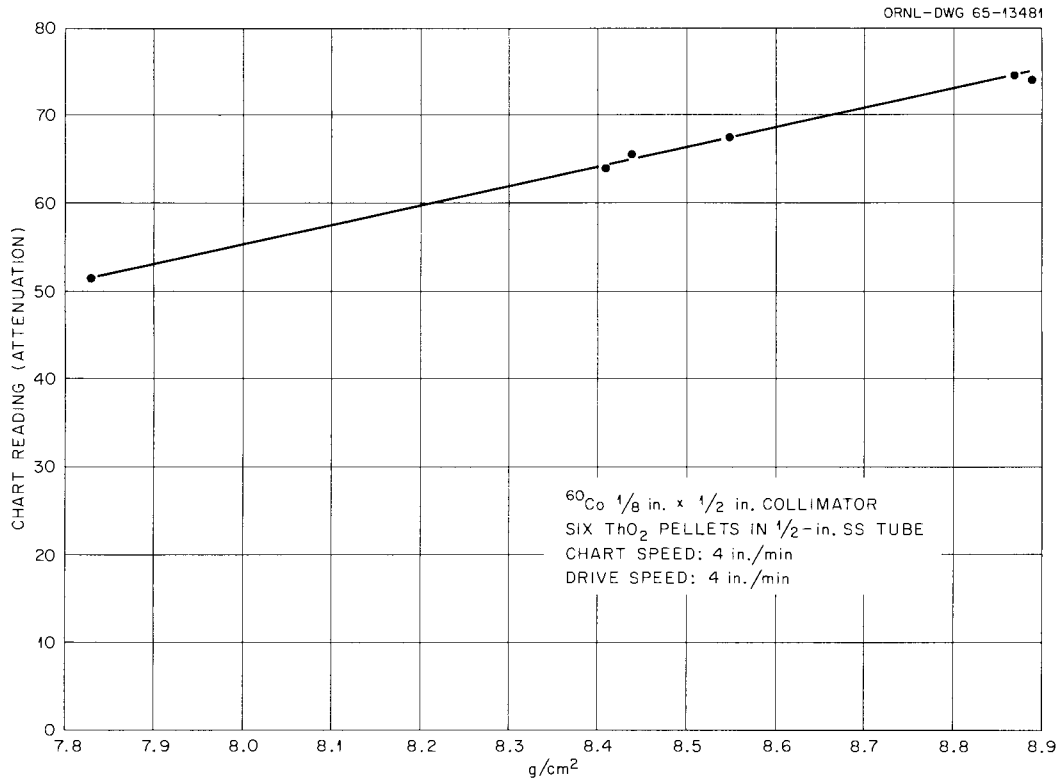


Fig. 4.5. Typical Calibration Chart Relating Fuel Content and Gamma Attenuation.

Stainless steel shims of 0.001 to 0.010-in. thickness are being placed on the 1/2- and 3/4-in.-diam ThO₂ pellets during scanning. The effect on gamma-ray attenuation by the different shim thicknesses will provide useful guideline information for specifying wall thickness tolerances of tubing used to house fuel pellets or vibratorily compacted fuel powders. The data analysis on this phase is incomplete.

5. ZIRCONIUM METALLURGY

M. L. Picklesimer

We are conducting research along several lines on zirconium-base alloys of potential use as structural materials for water-cooled and/or -moderated reactor systems. The principal projects are: (1) studies of the physical metallurgy, including transformation kinetics and morphologies, mechanical properties, phase diagrams, and heat-treatment response; (2) the development, evaluation, and utilization of preferred orientation and strain anisotropy in α -zirconium alloys during fabrication, and the utilization of yield stress anisotropy in increasing maximum permissible design stresses in structures; (3) the determination of the effects of composition, temperature, and environment on the oxidation-corrosion rates in the thin-film stages of oxide growth; (4) a study of the effects of alloy composition and oxidation environment on the structural properties of thin oxide films in situ; and (5) investigation of stress orientation of hydrides in Zircaloy-2.

Deformation, Creep, and Fracture in Alpha-Zirconium Alloys¹

M. L. Picklesimer

The anisotropy in mechanical properties observed in α -zirconium alloys can be related to the preferred orientation of the material. The anisotropy in yield strengths, plastic flow, creep, fracture, strain-rate and temperature sensitivities, and the stability of such textures to further deformation are discussed in terms of the texture and the deformation systems observed in single crystals. It is concluded that other deformation systems are forced to operate because of the restraint of neighboring grains in polycrystalline materials.

¹ Abstract of paper presented at a Symposium on Zirconium and Its Alloys, 1965 Fall Meeting of the Electrochemical Society, Buffalo, New York, October 10-14, 1965.

Research on the Mechanical Anisotropy of Zircaloy-2 (ref 2)

P. L. Rittenhouse

M. L. Picklesimer

The preferred orientation developed in close-packed hexagonal zirconium alloys during fabrication causes a strong anisotropy of plastic properties. A reliable system of evaluating and characterizing this anisotropy is a prerequisite to the use of zirconium alloys as materials of construction. Studies of the mechanical properties, strain behavior, and preferred orientation of Zircaloy-2 sheet were performed. A method was developed to describe the plastic anisotropy and preferred orientation using only the natural strain data from orthogonal pairs of tensile and compression specimens.

Effects of Neutron Irradiation and Vacuum Annealing
on Oxide Films on Zirconium³

J. C. Banter

Reflection and transmission spectra show no detectable effect of irradiation with a fast-neutron dose of 10^{19} neutrons/cm² on either oxide films on zirconium or on their rate of dissolution during vacuum annealing. However, the annealed films absorb light strongly throughout the spectral region from 2000 Å to 2.8 μ , apparently resulting from the production of defects by the film dissolution. Vigorous attack of the zirconium through annealed films by a solution of bromine in ethyl acetate supports the presence of defects, since unannealed specimens are unattacked. Other results indicate that estimates of film thicknesses on annealed specimens, based on visual observation of interference colors, may be appreciably in error. The importance of both film formation and oxygen dissolution to the overall oxidation mechanism is discussed.

²Abstract of paper presented at a Symposium on Zirconium and Its Alloys, 1965 Fall Meeting of the Electrochemical Society, Buffalo, New York, October 10-14, 1965.

³Abstract of paper presented at a Symposium on Zirconium and Its Alloys, 1965 Fall Meeting of the Electrochemical Society, Buffalo, New York, October 10-14, 1965.

Anisotropy in Zircaloy-2

P. L. Rittenhouse

M. L. Picklesimer

Zircaloy-2 Tubing

Two lots each of 1/2- and 3/4-in.-diam Zircaloy-2 tubing have been received from commercial vendors. Testing has begun on one lot of 3/4-in.-diam tubing with an 0.036-in. wall. Stress-strain curves for this tubing in uniaxial tension, uniaxial compression, and torsion are shown in Fig. 5.1. The mechanical property data are given in Table 5.1. The yield strengths predicted on the basis of the distortion energy condition for isotropic materials (using the uniaxial tensile yield strength as a base) are also given. The experimentally determined yield strengths in compression and torsion are appreciably higher than that predicted by the theory of isotropic materials.

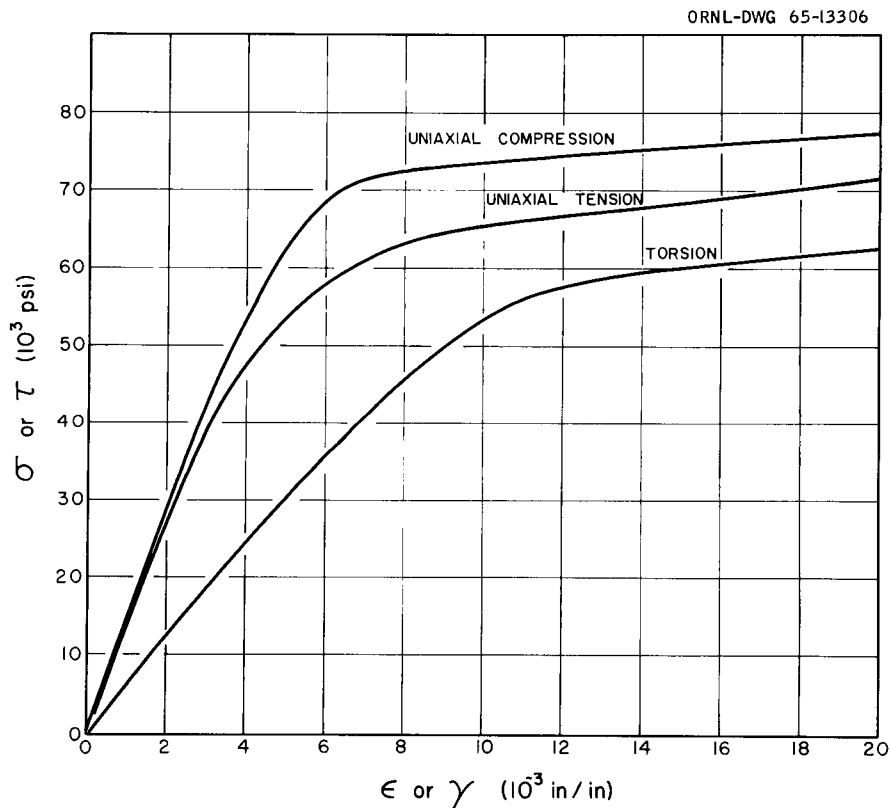


Fig. 5.1. Stress-Strain Curves for One Lot of 3/4-in.-diam Zircaloy-2 Tubing.

Table 5.1. Mechanical Properties of Zircaloy-2 Tubing

Test	Yield Strength, psi		Ultimate Tensile Strength (psi)	Elastic Modulus (psi)
	Experimental	Predicted		
	$\times 10^3$	$\times 10^3$	$\times 10^3$	$\times 10^6$
Tension	61.0	61.0	85.8	12.6
Compression	71.0	61.0		14.4
Torsion	56.0	49.8	70.0	6.2

The preferred orientation of the tubing was determined by a microhardness technique⁴ yielding the "average" basal pole figure shown in Fig. 5.2. Looking down the tube axis, as shown in Fig. 5.3, the basal poles are distributed equally with respect to the angle between the tangential and radial directions. An examination of the basal plane traces of many grains by the sensitive tint technique in a polarizing microscope⁵ showed texture variation across the wall to be negligible.

There are two distinctly different texture classes normally observed in Zircaloy-2 tubing. The first has the basal poles of the crystallographic texture concentrated parallel to the radius of the tube, and the second has them concentrated parallel to the circumferential direction. Materials of these textures will have plane stress yield ellipses of very different shape (i.e., their properties in biaxial stress will be appreciably different).⁶ Combinations of the two textures are common, and the yield properties of the material will vary with the relative magnitudes of each component. The material now being tested is expected to be a perfect intermediate in determining the relative contribution of each component to the overall yield behavior.

⁴P. L. Rittenhouse and M. L. Picklesimer, "Comparison of Pole Figure Data Obtained by X-Ray Diffraction and Microhardness Measurements on Zircaloy-2," accepted for publication in the Transactions of the Metallurgical Society of AIME.

⁵P. L. Rittenhouse and M. L. Picklesimer, Fuels and Materials Development Program Quart. Progr. Rept. June 30, 1965, ORNL-TM-1200, p. 35.

⁶P. L. Rittenhouse and M. L. Picklesimer, Fuels and Materials Development Program Quart. Progr. Rept. Dec. 31, 1964, ORNL-TM-1000, p. 70.

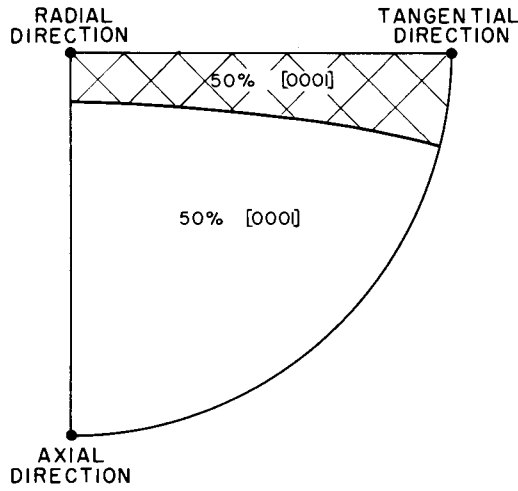


Fig. 5.2. Basal Pole Figure for the Tubing of Fig. 5.1. Determined by microhardness method.

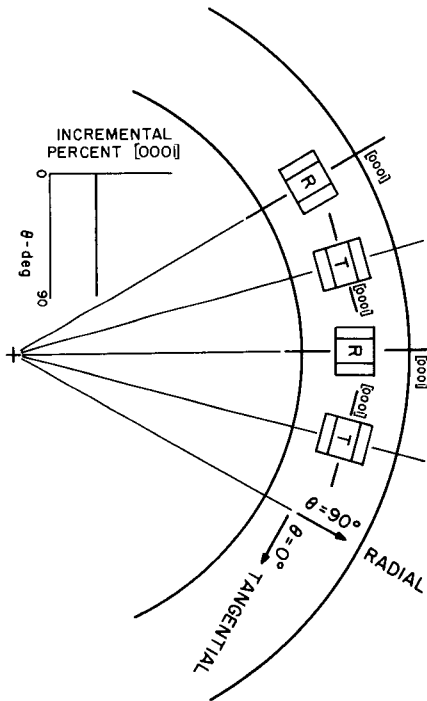


Fig. 5.3. Texture Gradient Through the Wall Tubing of Fig. 5.1.

Correlation of Yield Strengths with the "k" Values and Texture

Compression yield strengths and strain anisotropy in compression are being determined on the Zircaloy-2 plate and sheet materials previously studied in tension. The excellent empirical correlation obtained between "k" values in tension and in compression was described previously.⁷ At the present we are attempting to generate a quantitative relationship between the yield strengths of each material, their corresponding "k" values, and texture coefficients. It is easier to work with compression data, for there are three yield strength ratios available (the yield strengths are known in the rolling, transverse, and normal directions) as opposed to only one for each material in the case of tension. Many empirical correlations have been attempted, all show the same general trend, but none are as yet satisfactory. One such correlation, a plot of yield strength ratio as a function of a factor incorporating all six "k" values, is shown in Fig. 5.4.

⁷P. L. Rittenhouse and M. L. Picklesimer, Fuels and Materials Development Program Quart. Progr. Rept. Sept. 30, 1965, ORNL-TM-1270, p. 32.

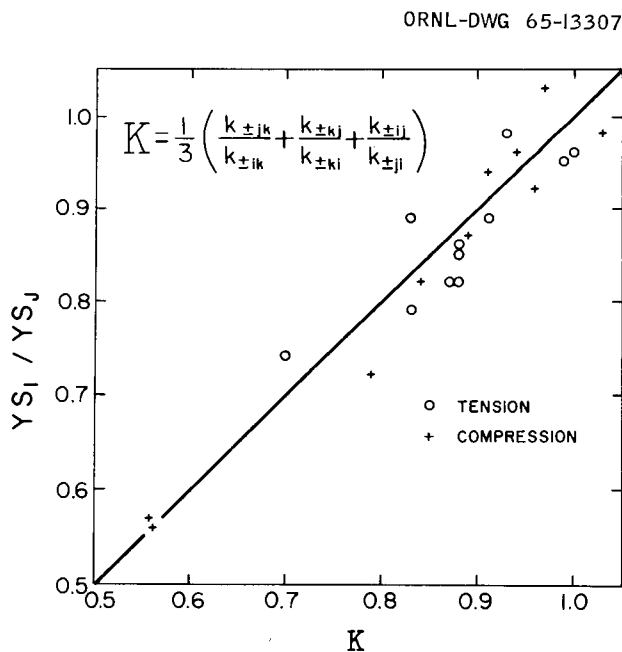


Fig. 5.4. Plot of the Ratio of Tensile and Compressive Yield Strengths as a Function of Strain Anisotropy Coefficients.

The 20 lots of sheet and plate material being tested are from 6 different primary sources. The normal variations in composition which undoubtedly exist (especially oxygen content) are enough to affect the yield strengths and, thereby, to complicate any correlations based on yield strengths. Only a small amount of the compression data is available, and it is felt that the chances are much better for obtaining a more quantitative correlation after the remainder of the data is obtained.

Determination of Yield Surfaces

A method of obtaining flow surfaces in stress space using the anisotropy of Knoop hardness measurements of zirconium alloys was described in a recent paper by R. G. Wheeler and D. R. Ireland.⁸ The surface determined is on the octahedral plane through the yield surface in stress space. After the yield locus is constructed on the octahedral plane, the known yield strength in some selected direction is equated with its corresponding position on the flow surface to calibrate that surface in terms of stress.

Flow surfaces determined by the hardness method for two of our Zircaloy-2 materials are shown in Fig. 5.5. The tensile and compressive yield strengths in the rolling direction were used to calibrate the stress surface. A comparison of the experimental and predicted yield strengths is given in Table 5.2. The prediction of yield strengths is quite good for Schedule 62 Zircaloy-2 but poor for Schedule 9. The compressive yield strength observed in the normal direction for Schedule 9 material is higher than predicted. Perhaps the major factor here is that the deformation may be forced to occur on a system or systems that need not be operative during deformation by the Knoop indenter. The predicted tensile yield strength in the normal direction (70,000 psi) is about the value we would expect from other data. Our next step will be to attempt to project various parts of these flow surfaces onto planes of biaxial stress to obtain portions of the plane stress yield ellipse for comparison with experiment.

⁸R. G. Wheeler and D. R. Ireland, "Multiaxial Plastic Flow of Zircaloy-2 Determined from Hardness Data," paper presented at a Symposium on Zirconium and Its Alloys, 1965 Fall Meeting of the Electrochemical Society, Buffalo, New York, October 10-14, 1965.

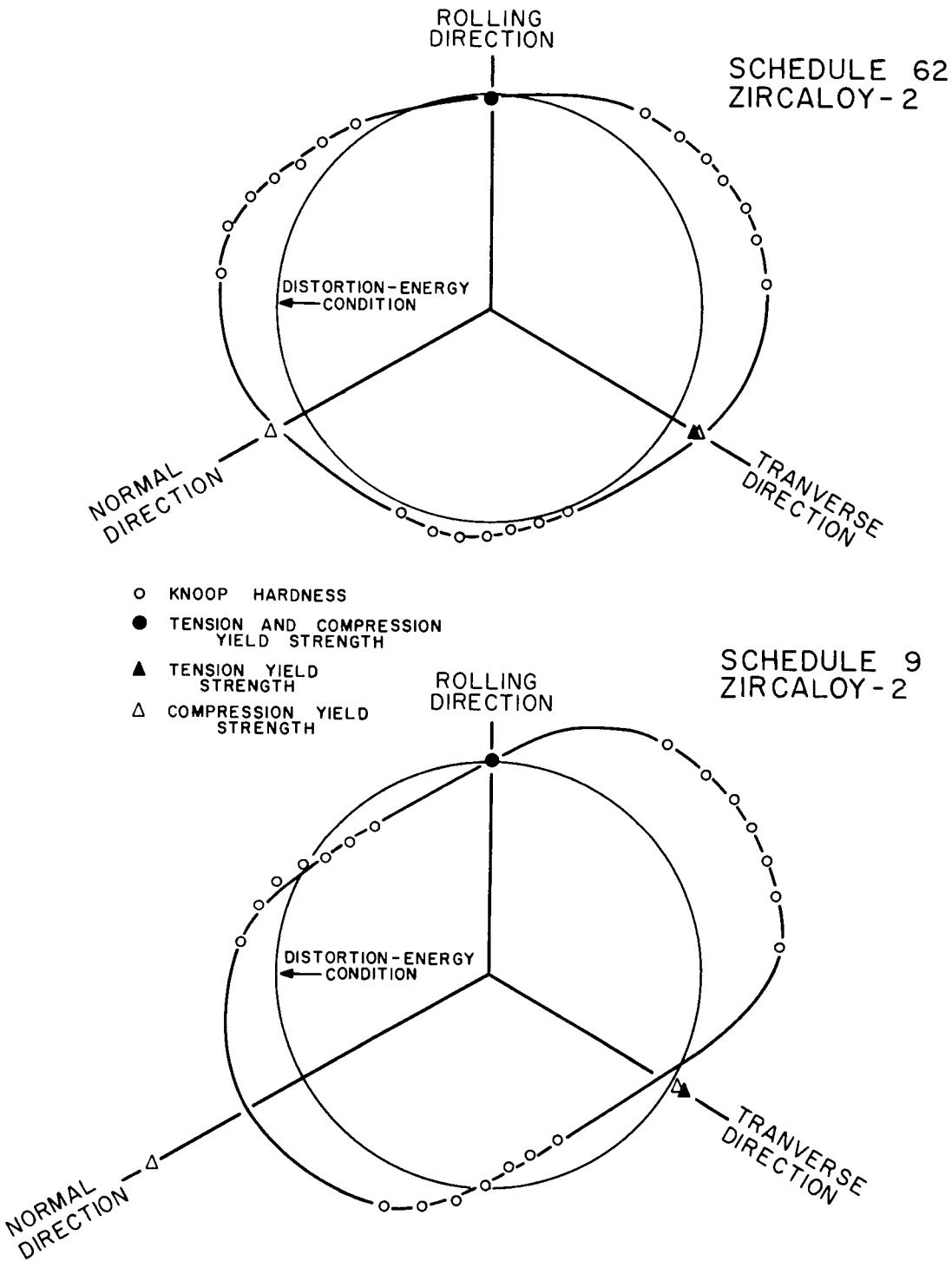


Fig. 5.5. Flow Surfaces in Stress Space as Determined by Hardness Anisotropy.

Table 5.2. Experimental and Predicted Yield Strengths

Schedule	Stress	Rolling Direction Yield Strength, psi		Transverse Direction Yield Strength, psi		Normal Direction Yield Strength, psi	
		Experimental	Predicted	Experimental	Predicted	Experimental	Predicted
		$\times 10^3$	$\times 10^3$	$\times 10^3$	$\times 10^3$	$\times 10^3$	$\times 10^3$
62	Tension	56	56	63	66		65
	Compression	69	69	79	81	82	80
9	Tension	55	55	58	52		70
	Compression	66	66	67	62	118	84

Oxide Film Studies

J. C. Banter

A compact, semiportable vacuum furnace has been designed to be coupled to the spectrophotometer and is presently under construction. This system will allow a study of the oxide films on zirconium by reflection techniques while they are at temperature during vacuum annealing for dissolution and during formation in thermal oxidation experiments. These experiments are expected to yield further information concerning the relative contributions of the oxide dissolution and formation processes to the oxidation behavior of zirconium.

A variable range electrometer has been used to measure the room-temperature electrical conductivity of anodically and air-formed oxide films on zirconium. This instrument eliminates the electrical breakdown of the films encountered in previous attempts to make such measurements.⁹ Preliminary measurements have shown that the electrical conductivity of the air-formed films is higher than that of the anodic films. These measurements will be extended to include specimens oxidized and vacuum annealed, and corroded in water and steam, as well as those of a wider range of anodizing voltages.

Purification of Zirconium

J. C. Wilson

Zone refining of crystal bar zirconium stock for purification and growth of single crystals is now routinely performed. Recently, iodide bars of titanium, hafnium, and vanadium have been zone melted and grown into single-crystal rods. Because of its high vapor pressure, the vanadium bar required considerable attention during melting.

⁹J. C. Banter, Fuels and Materials Development Program Quart. Progr. Rept. Sept. 30, 1965, ORNL-TM-1270, p. 42.

Preparation of Single Crystals of Zirconium
and Its Alloys

J. C. Wilson

Most of the grain growth occurring in single crystals of α -zirconium grown by the α - β - α cycling technique has been found to occur in the α phase. Zone-refined zirconium does not produce grains as large as iodide bar stock by the cycling technique, apparently because polygonization occurs and grain growth stops. A zone-melted single-crystal bar was produced having a $\langle 111 \rangle$ beta direction along the bar axis. It is being used to study the growth and transformation characteristics of zirconium crystals.

Properties of High-Purity Zirconium

J. C. Wilson

We are using high-purity single crystals of zirconium to study the fundamental nature of some of the more important phenomena in zirconium such as oxidation-corrosion behavior, plastic deformation, deformation modes, habit planes, morphology, and optical properties of zirconium hydrides.

Oxidation

We have previously shown the dependence of oxide film thickness¹⁰ on crystallographic planes in zirconium oxidized in air at 360°C (maximum film thickness, 600 Å). The same general pattern is followed in thicker films. The region around the basal pole of a zirconium single-crystal sphere oxidized for 200 hr at 400°C (after some hours at a lower temperatures) is shown in Fig. 5.6. From color comparisons with anodized strips, the oxide film thickness was judged to be about 7000 Å

¹⁰J. C. Wilson, Fuels and Materials Development Program Quart. Progr. Rept. March 31, 1965, ORNL-TM-1100, pp. 38-39.

PHOTO 82217

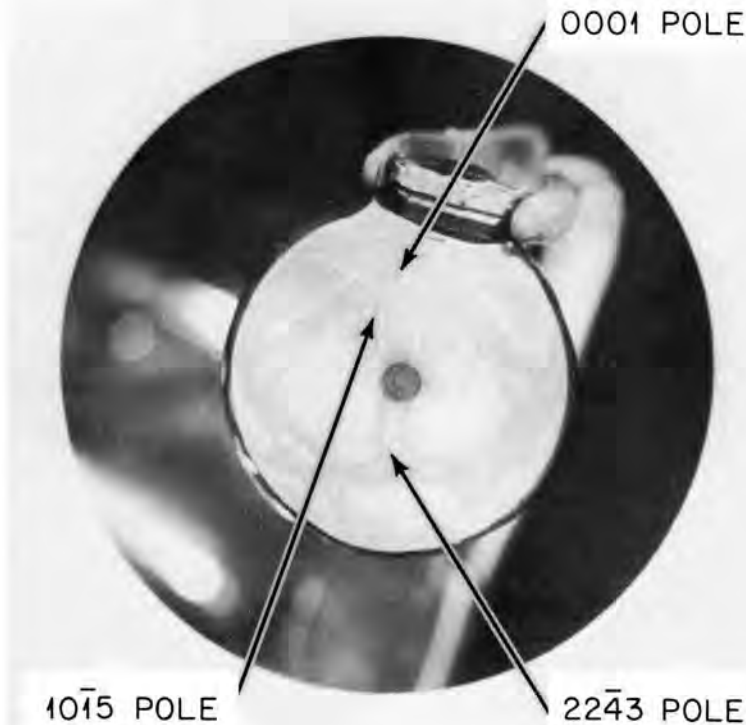


Fig. 5.6. Oxidation Anisotropy on a Single-Crystal Sphere of Zirconium Oxidized in Air for 200 hr at 400°C. Film thickness at the basal pole is approximately 7000 Å and 1700 Å near $\{10\bar{1}5\}$. Four orders of green interference color can be seen by visual examination. The dark circle in the center is a reflection of the camera lens.

at the basal pole and about 1700 Å near the $\{10\bar{1}5\}$ pole. There is, then, about a 4 to 1 variation in oxide film thickness with crystallographic direction; this variation can occur for an orientation difference of only 20° [the angle between (0001) and $\{10\bar{1}5\}$].

The deformation and annealing textures of rolled zirconium and of many of its alloys usually consist of a large number of grains with basal poles within about 30° of the normal direction. Because of the variation in oxide thickness observed, it is to be expected that there will be significant differences in oxidation behavior in polycrystalline materials differing only slightly in texture orientation and intensity.

If the dissolution of oxide films into zirconium shows the same 4 to 1 variation as does oxidation, as might be expected from the data of Pemsler,¹¹ the dissolution of anodized films of equal thickness will lead to wide, grain-to-grain color variations in polycrystalline materials. These color variations will not be seen in the anodized films as formed, because most anodizing processes produce little thickness variation with crystal orientation. As dissolution occurs, the thickness of the oxide film on each grain will be dependent on the crystallographic orientation of that grain surface, and the interference maxima and minima observed in reflection spectrophotometry will be smeared out, and make it difficult to measure the average film thickness by optical methods.

The anisotropy of oxidation in zirconium during anodizing in a 1% KOH solution was determined on a single-crystal sphere at potentials ranging from 5 to 80 v. The films produced have a thickness factor of about 29 A/v. The pattern of anodic oxidation is, at first, quite similar to that found for air oxidation,¹⁰ but it is more regular in outline, with some details being distinctly different. Above about 50 v (1500-A-thick film), the pattern tends to reverse itself in color gradient; the regions having the thinner films at lower voltages have the thicker films at the higher voltages. In no case was there greater than a 2 to 1 variation in thickness with orientation and this occurred only at low voltages. At 80 v (about 2300 A) there was no more than a 20% difference in thickness between the thickest and thinnest section of the anodic oxide film.

Hydrides in Zirconium

We are studying the habit planes, morphology, optical properties, and distribution of hydrides in both single- and polycrystalline zirconium, since the hydrides affect the mechanical properties of

¹¹J. P. Pemsler, The Diffusion of Oxygen in Zirconium and Its Relation to Oxidation and Corrosion, NMI-1177 (1957).

zirconium and its alloys. The commonly used chemical and electro-polishing solutions for zirconium have been found to attack either the hydrides, the adjacent metal, or both. An electropolishing solution of 15% by volume of perchloric acid (specific gravity 1.65) in ethanol produces an excellent electropolish at 25 v at -45 to -55°C for metallography at high magnification. Little preferential attack of the hydride or matrix occurs, the zirconium-iron intermetallics are preserved, and the grain boundaries are only slightly etched. A very rapid chemical polish that does not selectively remove hydrides, or the metal adjacent to them, consists of a solution of 10% by volume of concentrated (48%) HF in water. The reaction is violent and a chemical polishing time of only a few seconds is usually sufficient.

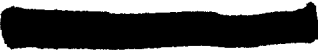
By the use of the above solutions, we have been able to examine the hydrides in relation to the metal matrix, rather than that of surface depressions where the hydrides have been. The hydrides have been found to show optical anisotropy in polarized lights, even in slowly cooled specimens. The optical anisotropy gives a possible tool for determining hydride crystal orientation relative to the matrix during microscopic examination.

A series of crystal-bar and zone-refined zirconium specimens hydrided to 0 to 500 ppm H_2 have been given various thermal and mechanical treatments. The following tentative observations can be made at this time: (1) hydrides not on the prism planes are most often observed near the surface of the metal or they are found to intersect hydrides that are on the $\{10\bar{1}0\}$ planes. The intersections seem to occur only at the midpoint or at one end of the hydride on the $\{10\bar{1}0\}$ plane. (2) Hydride plates viewed on edge are rarely straight, and if platelets nearly parallel to the plane of observation are carefully polished away, the metal surface underneath appears to be ruffled. (3) Large hydride plates are usually thickened where they intersect grain boundaries. (4) Grain boundary hydrides are rarely observed in zone-refined zirconium. (5) The hydride plates seem to have a fine structure within them, perhaps from twinning, or deformation. (6) The optical anisotropy of the hydrides on prism planes is quite small when looking at a basal

plane in zirconium; this suggests that the optical axis of the hydride is near that of the zirconium matrix. This seems logical since the "c" lattice parameters of zirconium and the γ' hydride are within a few percent of each other.

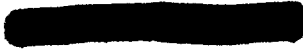
[REDACTED]

[REDACTED]



PART II

REACTOR CHEMISTRY DIVISION



[REDACTED]

[REDACTED]

6. FISSION-GAS RELEASE AND PHYSICAL PROPERTIES OF
FUEL MATERIALS DURING IRRADIATION

R. M. Carroll O. Sisman

This is the third reporting of a program that is newly sponsored by the Reactor Fuels and Materials Development Branch. The first two reports^{1,2} were used to give the background, experimental methods, and a summary of our observations and conclusions. In brief, we are studying the release of fission gas from UO_2 during irradiation in an effort to determine the fundamental mechanism by which the gas migrates and escapes from the fuel. To accomplish this we irradiate carefully-selected and characterized specimens in an irradiation facility where the neutron flux and temperature is controlled independently. Fission gas is entrained in a constantly moving stream of sweep gas and carried outside the reactor where it is analyzed by gamma-ray spectrometry

As a result of these studies, we believe that the fission gas is released by a combination trapping and diffusion process where the trapping is the dominant factor determining the time required for the gas to escape. We have formed a defect-trap theory that postulates that defects in the UO_2 crystal structure will trap migrating xenon and krypton atoms.³ Some defects are naturally present in the UO_2 , and others can be formed by irradiation. The irradiation-formed defects start as point defects which can vanish by annealing but may cluster to form larger defects that will require longer times to anneal.

The gas escape from a UO_2 specimen thus depends on the initial condition of the specimen, the temperature, fission rate, and the previous irradiation conditions of the specimen. We have made a

¹R. M. Carroll and O. Sisman, Fuels and Materials Development Program Quart. Progr. Rept. June 30, 1965, ORNL-TM-1200, pp. 55-64.

²R. M. Carroll and O. Sisman, Fuels and Materials Development Program Quart. Progr. Rept. Sept. 30, 1965, ORNL-TM-1270, pp. 49-59.

³R. M. Carroll and O. Sisman, Nucl. Sci. Eng. 21, 47-58 (1965).

mathematical formulation of this theory.⁴ To obtain values for the parameters of the mathematical model, we have included dynamic testing wherein either fission rate or temperature is cyclically perturbed while the other is maintained constant. Also, the mass of data resulting from the dynamic program requires computer processing. Thus, the majority of the data must be taken in a punch tape format. The net result is that a combination of complex instrumentation must be working over the period of the test and the misbehavior of one component will void the test. The testing of the specimen during the time of this report was mainly regarded as a period to develop the technique, instruments, computer program and generally to solve the problems associated with dynamic testing. These problems have all been resolved satisfactorily and some useful information has been obtained from the UO₂ single crystal now being tested.

Uranium Dioxide Single-Crystal Specimen, Cl-18

Two single-crystal disks were sandwiched together in an Al₂O₃ holder with thermocouples between them and pressing against their outer surfaces (Fig. 6.1). These UO₂ specimens were polished to a metallographic finish before irradiation to minimize surface defects. The physical characteristics are given in Table 6.1. The crystal orientation, in relation to the faces of the disk, was determined by x-ray diffraction and a pair of crystals with the same orientation was selected. The polished crystal was examined with the optical microscope for visible defects and none were found. By chemical analysis of disks A and B the oxygen-to-uranium ratio was < 2.001, and the major impurity contents in parts per million were: C, < 20; N, 63; F, 140; Fe, 150; Ca, 100; Si, 10; and Mg, 20.

⁴R. M. Carroll, R. B. Perez, and O. Sisman, J. Am. Ceram. Soc. 48(2), 55-59 (1965).

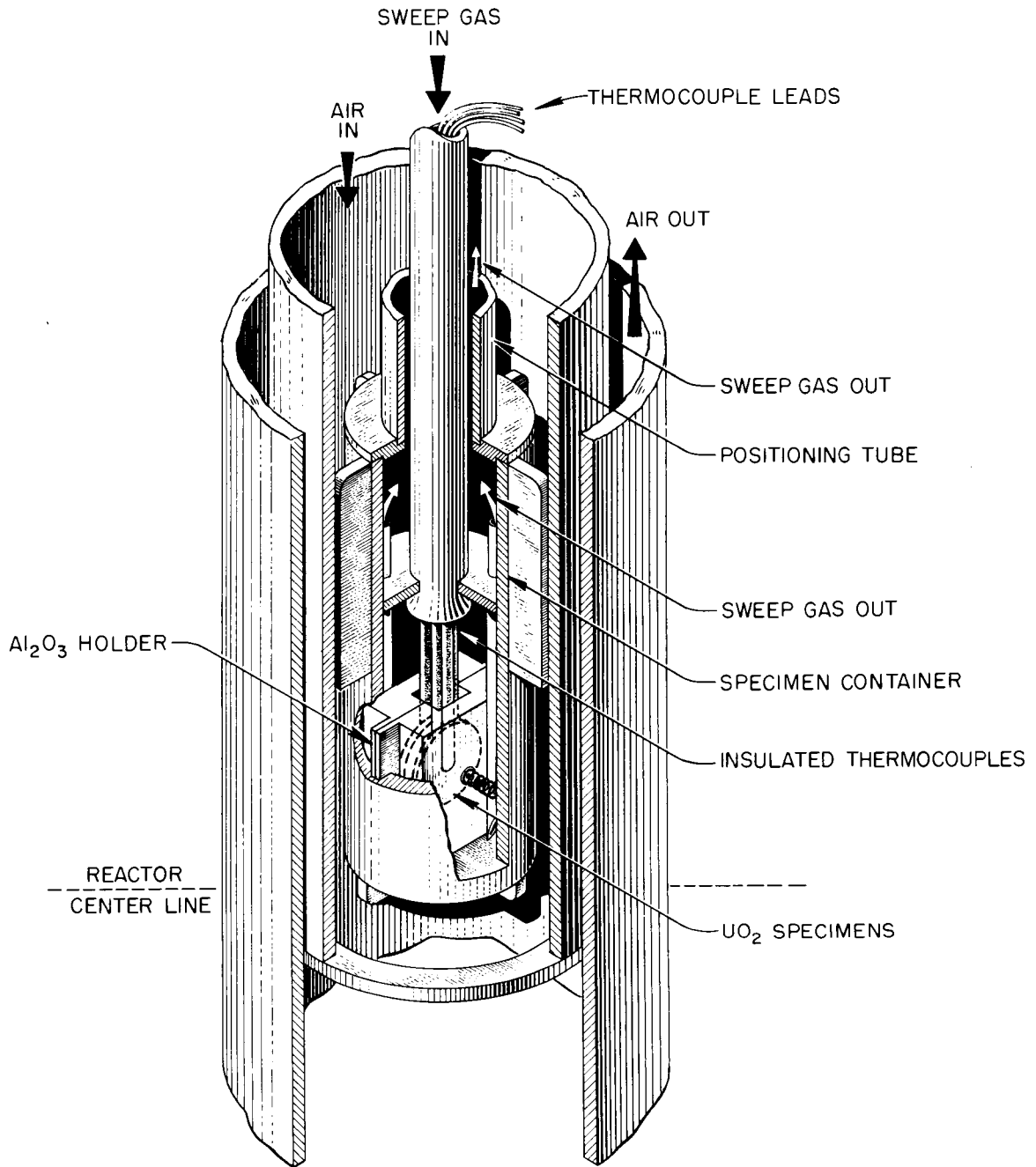


Fig. 6.1. Capsule Arrangement, Polished Single Crystals of UO₂.

Table 6.1. Uranium Dioxide Single Crystal Cl-18 Characteristics
(Two Single-Crystal Disks in Capsule Cl-18, As Polished.)

Disk	Weight (g)	Thickness (cm)	Diameter (cm)	Density (g/cm ³)	Crystal Orienta- tion	Visible Defects (micro- scopic)
A	0.8225	0.0599	1.269	10.86	(110) 1°	None
B	0.9763	0.0714	1.266	10.87	(110) 0.95°	None

Fission-Gas Release (Steady State)

Previous to the Cl-18 polished single crystal, another polished single crystal (Cl-13) was irradiated. The physical characteristics of the specimens were nearly identical, but the fission-gas release was somewhat different between the two specimens (see Fig. 6.2). The low-temperature release shown in Fig. 6.2 is much higher for the Cl-18 crystals than for the previous polished crystals. In Fig. 6.2 it appears that the temperature dependence of the gas release from the Cl-18 crystals is less than that from the Cl-13 crystals; however this is only an illusion caused by the different low-temperature release rates. If the low-temperature release rates are subtracted, then the temperature dependence of the gas release is the same (Fig. 6.3), although the amounts of gas released are different. The different neutron fluxes do not account for the different rates of gas release from the two specimens (the gas release is not responsive to changes of neutron flux).^{1,2}

The fission-gas release from the two sets of polished single-crystal specimens is significantly different than the gas release from other specimens we have tested. Therefore, we will list these differences below and discuss the possible causes.

Low-Temperature Release

When unpolished single-crystal specimens were irradiated, we observed that the low-temperature (as well as the high-temperature) release rate decreased exponentially as burnup progressed.³ We believe that the low-temperature release is caused by a knockout process

ORNL-DWG 65-13319

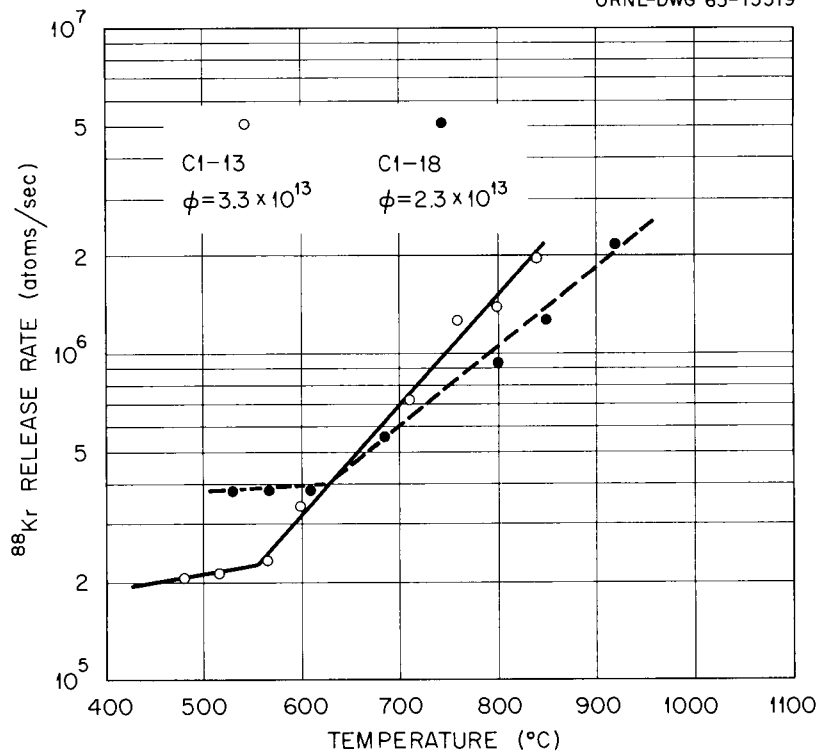


Fig. 6.2. Comparison of ^{88}Kr Release from Single-Crystal UO_2 Specimens C1-13 and C1-18.

ORNL-DWG 65-13322

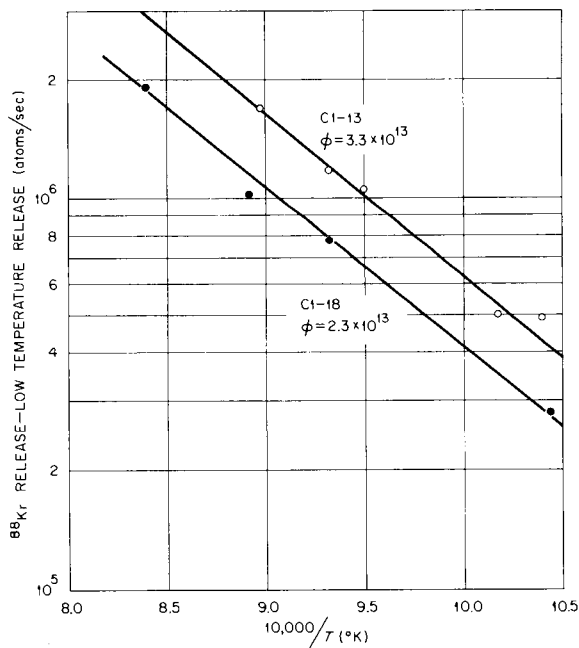


Fig. 6.3. Krypton-88 Release when Low-Temperature Release is Subtracted.

whereby UO_2 molecules are ejected from the surface by emerging fission fragments. Naturally, gas atoms in the vicinity are also ejected. The amount of knockout depends on the total surface area of the UO_2 specimen, and we think that the decrease of the low-temperature release is caused by irradiation smoothing of the specimen surface. We have found that a single crystal is smoother after irradiation.³ To test this theory, we polished the surface of the crystals to the smoothest surface we could obtain, reasoning that an already smooth surface would show very little additional smoothing.

Both sets of polished single crystals showed no change of low-temperature gas release as burnup progressed; thus supporting our smoothing theory. However, the low-temperature release of fission gas was different between the specimens, with Cl-18 having a much higher release than Cl-13 (Fig. 6.4). The low-temperature gas release of unpolished specimens Cl-9 is also shown in Fig. 6.4 after these specimens became smoothed by irradiation.

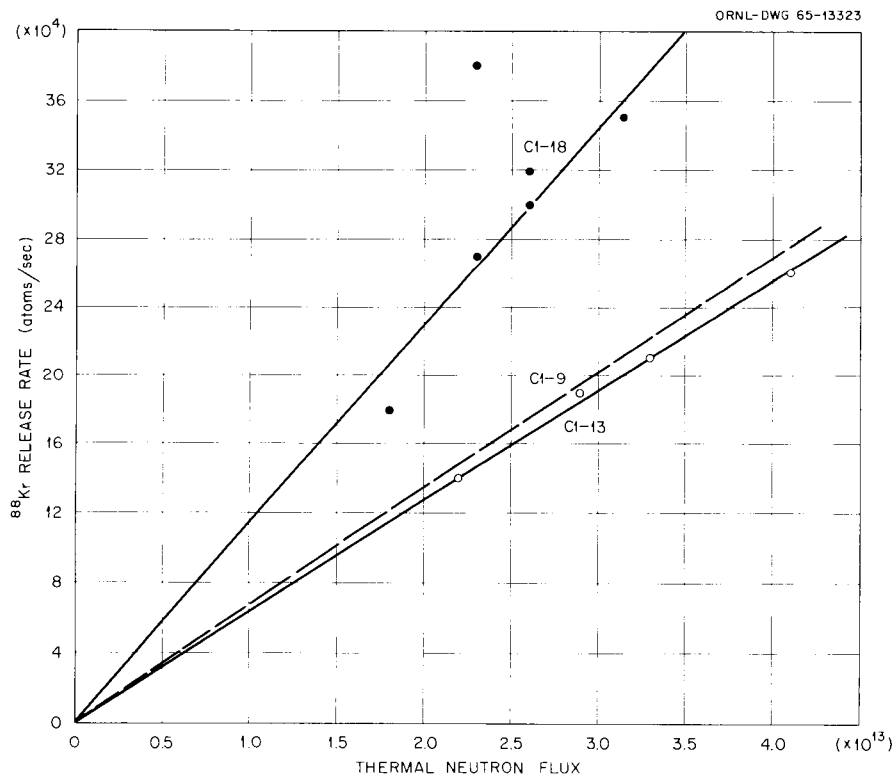


Fig. 6.4. Comparison of ^{88}Kr Temperature Independent Release Between Single-Crystal UO_2 Specimens of the Same Size.

The higher release rate of specimens Cl-18 (Fig. 6.4) can be explained in two ways. (1) The surface of Cl-18 was larger than Cl-13. This seems unlikely since the Cl-18 surface would have to be twice as large as the Cl-13 to produce this result. Such a difference should have been apparent from microscopic examinations. (2) The crystal orientation of the UO_2 crystals (in relation to the surface of the disk) was different, (110) 1° for Cl-18 and (100) 18° for Cl-13. It may be that more knockout can occur in one orientation than another. Also it is possible that the fission fragments and other energetic particles could become somewhat focused by the crystal planes and travel greater distances within the UO_2 before being stopped. This would cause more knockout since more fission fragments would penetrate the surface.

High-Temperature Release

The fission-gas release from the polished single-crystal specimens was different from what we had observed previously. With unpolished single crystals³ and fine-grain specimens⁵ the gas release increased exponentially with temperature above about $600^\circ C$ (see Fig. 6.5). We found that the gas release from the polished crystals was exhibiting two behavior patterns hitherto unobserved; a deviation from the exponential increase with temperature and a thermal history dependence.

The ^{88}Kr release rate from the polished single-crystal (Cl-18) specimens is given in Fig. 6.6. The distinguishing feature between Figs. 6.5 and 6.6 is that a relatively straight line can be drawn through the high-temperature data points (on a log plot) of Fig. 6.5 while a distinct deviation at about $950^\circ C$ occurs on Fig. 6.6. This deviation is greatest at about $1050^\circ C$ and appears in all our measurements in the temperature range between 900 and $1100^\circ C$. Above $1150^\circ C$ the gas release continues to increase exponentially with temperature as would be expected.

⁵R. M. Carroll and O. Sisman, J. Nucl. Materials 17(4), 305 (1965).

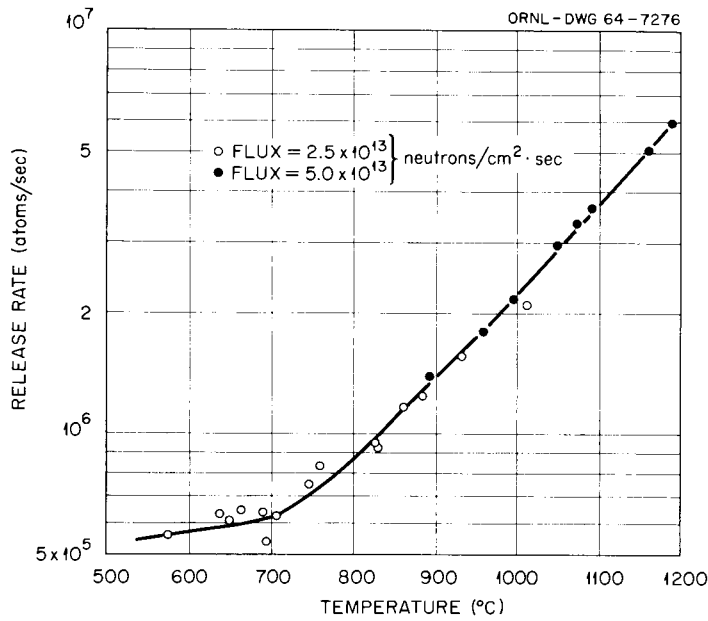


Fig. 6.5. Release Rate of ^{88}Kr from Fine Grain Specimen (Cl-12) of UO_2 .

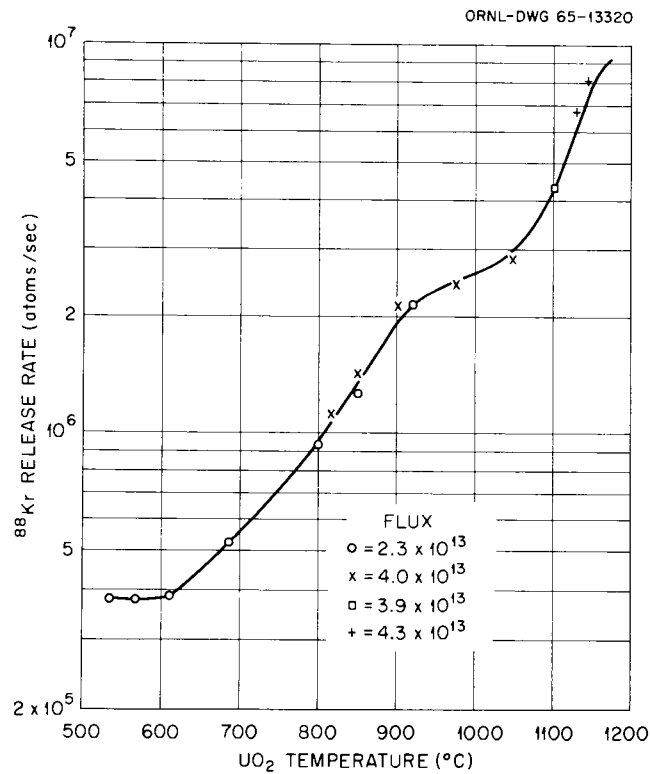


Fig. 6.6. Uranium Dioxide Single-Crystal Cl-18 Temperature Dependence of ^{88}Kr Release.

This high-temperature dip was not present in the fine-grain specimens (Fig. 6.5); and we had not previously recognized it in the unpolished single-crystal specimens, mainly because only one previous single-crystal specimen (unpolished) was irradiated at temperatures over 1000°C. By examining the gas release from this previous data a small dip can be observed, much less than from the polished crystals. Also, the polished single crystal (C1-13) showed a significant deviation at the highest range of measurements. At the time, we speculated this was thermocouple problems, since only one datum point was involved (see Fig. 6.7, line C1-13).

We believe that this deviation from an exponential release of fission gas with temperature is because, at a temperature range of 950 to 1100°C, point defects cluster at an increased rate. We think these clusters are rather uniform in size, less than 100 Å in diameter, and anneal slower than do the smaller point defects. The clusters are also traps and the point defect that enters the cluster will exist longer than it would as a free point defect.

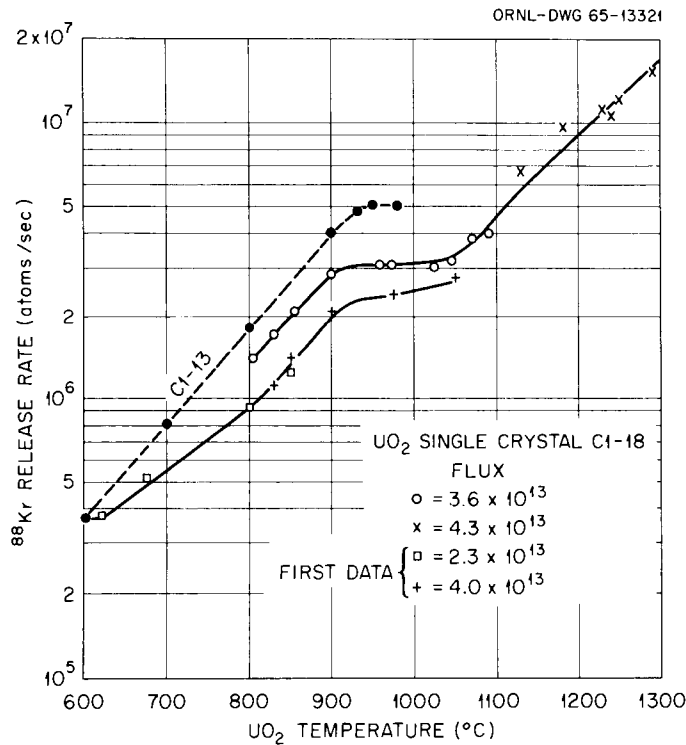


Fig. 6.7. Krypton-88 Release from UO_2 Single Crystal as a Function of Temperature and History.

Assuming a uniform rate of production of point defects, as the temperature increases the free lifetime of the point defect decreases causing the trapping cross section of the point defects to decrease. Above 900°C, clustering becomes significant and as the temperature increases the trapping cross section of clusters increases, compensating for the decreasing point defects. The gas release then does not increase with temperature in this temperature range.

At higher temperatures the point defects are of much less importance as traps than are clusters, but the clusters are now annealing at a greater rate. Thus, as the temperature continues to increase the clusters anneal at a faster rate reducing the trapping probability and the fission-gas escape again increases exponentially with temperature.

The effect of clustering is more apparent when the UO₂ specimen initially has only a small amount of defects in the crystal structure. The fine grain specimen had a high concentration of defects because of the grain boundaries and the additional defects added by the clusters (if they occurred) would not be detected. It is quite possible that the point defects were captured by the grain boundaries in the fine-grain specimen and the clusters never formed.

Temperature History Dependence. - Although some specimens in the past have shown a burnup effect,³ we had never detected an effect caused by temperature history. The defect-trap theory predicts that when clusters are formed they will affect the subsequent gas-release rate. However, the clusters are apparently not formed until the UO₂ temperature is at about 1000°C and only a few of the specimens have been irradiated above that temperature. Thus, the temperature history effect would (1) be caused by clustering of point defects, (2) would not occur until the temperature was above about 1100°C, and (3) at least some of the effect would anneal in subsequent irradiations. The effect of history dependence is shown in Fig. 6.8 where four sets of data separate into two parts, the initial portion of the irradiation and the subsequent portions, after operating at temperatures above 1000°C.

The history dependence is not observed if the specimen is operated at temperatures below 1000°C. If the specimen is irradiated at temperatures higher than 1000°C for several days and then irradiated at lower

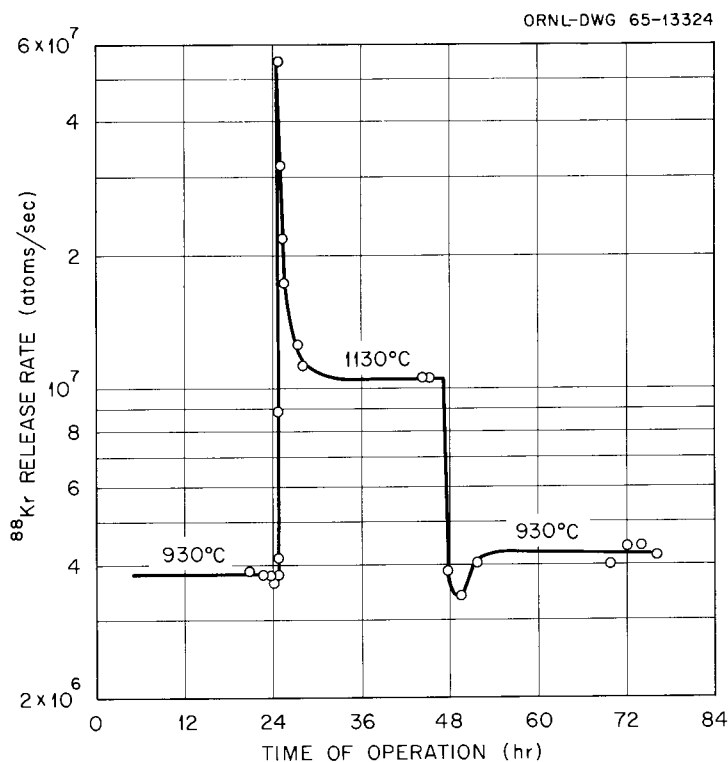


Fig. 6.8. Krypton-88 Release Rates when Single-Crystal UO_2 (Cl-18) Temperatures were Changed.

temperatures, the gas release will be somewhat higher than expected. We cannot offer a good explanation of this phenomenon now, but it is probably a consequence of the annealing of the clusters formed at the higher temperatures because after some time the gas release will return to its original level.

The history dependence of the gas release is illustrated in Fig. 6.8 where the specimen temperature was increased from 930 to 1130°C and after about 24 hr returned to 930°C. The gas release was about 13% higher after the 1130°C temperature. The dip in the gas-release rate as the specimen cooled was likely caused by momentarily cooling the specimen lower than 930°C.

Oscillations of Neutron Flux

We have found that the low-temperature flux oscillations do increase the average release.⁶ One question was whether the neutron flux oscillations would change the average magnitude of the gas-release rate at high temperatures. To determine this, we took samples of gas during neutron flux oscillations at constant temperature and cycle frequencies ranging from 20 to 400 min. Sixty different gas samples were analyzed during these oscillations and we could find no effect of frequency of oscillation on the average amount of gas released at temperatures above 900°C.

Temperature Oscillations

The temperature is difficult to control during flux oscillations and sometimes a small amplitude, high frequency, temperature oscillation occurs when a steady temperature is desired. A series of measurements were made by first using manual control of temperature and then maintaining the same temperature with automatic control (producing the high frequency vibration) to see if this small vibration of temperature affected the gas release. The results of this test showed that manual and automatic control both produced the same gas-release rate.

Gas-Transfer Functions

High-frequency waves of fission-gas release cannot be measured if the waves become mixed during the time required to move the gas to the analysis point. We studied gas mixing by injecting argon into the capsule of a full-scale model of the sweep-gas system. The wave form of the argon concentration in the helium sweep was measured by a thermal-conductivity gas-chromatographic apparatus. The sweep velocity was measured by liquid displacement.

⁶R. M. Carroll and O. Sisman, Fuels and Materials Development Program Quart. Progr. Rept. Sept. 30, 1965, ORNL-TM-1270, pp. 49-59.

We define a mixing factor as the length of time an instantaneous pulse of argon could be detected at the sampling point because of mixing in the sweep gas. For example, argon could be added to the sweep stream for 3 min, and it would later be detected over a period of 12 min. The mixing factor would be 9 min. If argon were then added for 1 min, the detection period would be 10 min, and so on. The mixing factors varied according to the sweep flow rate and this relation is shown in Fig. 6.9. This curve will allow us to choose the proper sweep gas flow rate to obtain optimum results from a given oscillation program.

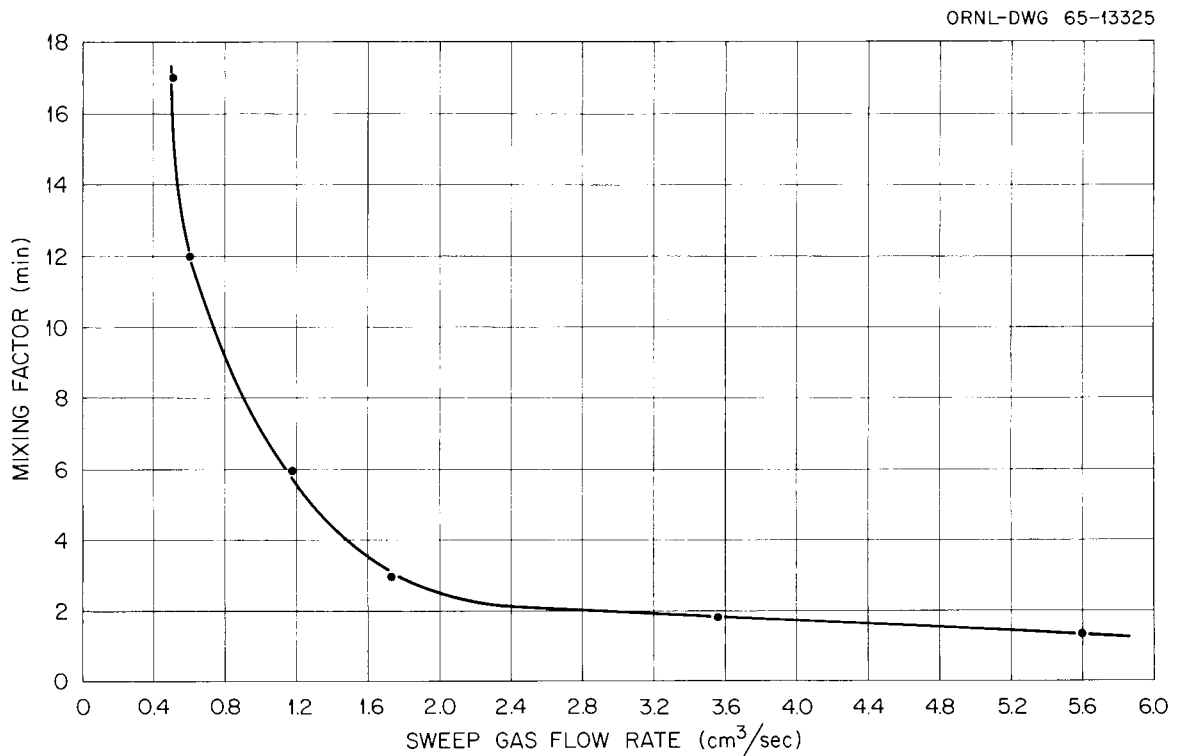


Fig. 6.9. Mixing Factor in C-1 Experiment as a Function of Sweep Gas Flow Rate.

Previous reports in this series are:

ORNL-TM-920	Period Ending June 30, 1964
ORNL-TM-960	Period Ending September 30, 1964
ORNL-TM-1000	Period Ending December 31, 1964
ORNL-TM-1100	Period Ending March 31, 1965
ORNL-TM-1200	Period Ending June 30, 1965
ORNL-TM-1270	Period Ending September 30, 1965

Internal Distribution

- | | | | |
|--------|-------------------------------|------|--------------------|
| 1-3. | Central Research Library | 61. | C. F. Leitten, Jr. |
| 4-5. | ORNL - Y-12 Technical Library | 62. | A. L. Lotts |
| | Document Reference Section | 63. | R. N. Lyon |
| 6-15. | Laboratory Records | 64. | H. G. MacPherson |
| 16. | Laboratory Records, RC | 65. | R. E. MacPherson |
| 17. | ORNL Patent Office | 66. | M. M. Martin |
| 18. | G. M. Adamson, Jr. | 67. | W. R. Martin |
| 19. | J. C. Banter | 68. | D. I. Matkin |
| 20. | J. H. Barrett | 69. | R. W. McClung |
| 21. | S. E. Beall | 70. | H. E. McCoy, Jr. |
| 22. | R. J. Beaver | 71. | H. C. McCurdy |
| 23. | M. Bender | 72. | R. E. McDonald |
| 24. | R. G. Berggren | 73. | D. L. McElroy |
| 25. | J. O. Betterton, Jr. | 74. | C. J. McHargue |
| 26. | D. S. Billington | 75. | F. R. McQuilkin |
| 27. | A. L. Boch | 76. | A. J. Miller |
| 28. | B. S. Borie | 77. | E. C. Miller |
| 29. | G. E. Boyd | 78. | F. H. Neill |
| 30. | W. H. Bridges | 79. | S. M. Ohr |
| 31. | R. B. Briggs | 80. | M. F. Osborne |
| 32. | W. E. Brundage | 81. | P. Patriarca |
| 33. | R. M. Carroll | 82. | F. H. Patterson |
| 34. | J. V. Cathcart | 83. | A. M. Perry |
| 35. | G. W. Clark | 84. | S. Peterson |
| 36. | K. V. Cook | 85. | M. L. Picklesimer |
| 37. | J. H. Crawford | 86. | P. L. Rittenhouse |
| 38. | J. E. Cunningham | 87. | W. C. Robinson |
| 39. | J. H. DeVan | 88. | M. W. Rosenthal |
| 40. | C. V. Dodd | 89. | G. Samuels |
| 41. | D. A. Douglas, Jr. | 90. | J. L. Scott |
| 42. | J. I. Federer | 91. | O. Sisman |
| 43. | B. E. Foster | 92. | G. M. Slaughter |
| 44. | A. P. Fraas | 93. | G. P. Smith, Jr. |
| 45. | J. H. Frye, Jr. | 94. | S. D. Snyder |
| 46. | R. J. Gray | 95. | I. Spiewak |
| 47. | W. R. Grimes | 96. | J. T. Stanley |
| 48. | H. D. Guberman | 97. | W. J. Stelzman |
| 49. | J. P. Hammond | 98. | J. O. Stiegler |
| 50. | W. O. Harms | 99. | A. Taboada |
| 51. | R. L. Heestand | 100. | D. B. Trauger |
| 52-53. | M. R. Hill | 101. | J. T. Venard |
| 54. | N. E. Hinkle | 102. | G. M. Watson |
| 55. | H. W. Hoffman | 103. | M. S. Wechsler |
| 56. | H. Inouye | 104. | A. M. Weinberg |
| 57. | T. N. Jones | 105. | J. R. Weir, Jr. |
| 58. | G. W. Keilholtz | 106. | W. J. Werner |
| 59. | B. C. Kelley | 107. | G. D. Whitman |
| 60. | J. A. Lane | 108. | J. M. Williams |

109. R. O. Williams
 110. J. C. Wilson
 111. H. L. Yakel, Jr.
112. F. W. Young, Jr.
 113. C. S. Yust

External Distribution

- 114-116. F. W. Albaugh, GE, Hanford
 117. R. J. Allio, Westinghouse Atomic Power Division
 118. R. D. Baker, Los Alamos Scientific Laboratory
 119. L. Brewer, University of California, Berkeley
 120. V. P. Calkins, GE, NMPO
 121. W. Cashin, Knolls Atomic Power Laboratory
 122. S. Christopher, Combustion Engineering, Inc.
- 123-124. D. F. Cope, AEC, Oak Ridge Operations
 125. G. K. Dicker, Division of Reactor Development, AEC,
 Washington
126. E. A. Evans, GE, Vallecitos
 127. W. C. Francis, Phillips Petroleum Company
 128. R. G. Grove, Mound Laboratory
 129. D. H. Gurinsky, BNL
 130. S. Hasko, NBS
 131. A. N. Holden, GE, APED
- 132-134. J. S. Kane, University of California, Livermore
 135. J. H. Kittel, ANL
 136. E. J. Kreih, Westinghouse, Bettis Atomic Power Laboratory
 137. W. L. Larsen, Iowa State University, Ames Laboratory
 138. J. H. MacMillan, Babcock and Wilcox Company
 139. R. E. Pahler, Division of Reactor Development, AEC,
 Washington
140. S. Paprocki, BMI
 141. D. Ragone, GA
 142. Division of Research and Development, AEC, ORO
 143. A. H. Roberson, U. S. Department of the Interior,
 Bureau of Mines
 144. W. Rostoker, Illinois Institute of Technology
 Research Institute
 145. F. C. Schwenk, Division of Reactor Development, AEC,
 Washington
- 146-147. J. M. Simmons, Division of Reactor Development, AEC,
 Washington
 148. L. E. Steele, Naval Research Laboratory
 149. R. H. Steele, Division of Reactor Development, AEC,
 Washington
150. W. F. Sheely, Division of Research, AEC, Washington
 151. A. Strasser, United Nuclear Corporation
 152. W. R. Voigt, Division of Reactor Development, AEC,
 Washington
 153. C. E. Weber, Atomics International
 154. G. W. Wensch, Division of Reactor Development, AEC,
 Washington
 155. M. J. Whitman, Division of Reactor Development, AEC,
 Washington
- 156-170. Division of Technical Information Extension